Coordination Chemistry Reviews 253 (2009) 2493–2514

Contents lists available at ScienceDirect

Coordination Chemistry Reviews

journal homepage: www.elsevier.com/locate/ccr

Review

Iron(II) complexes of 2,6-di(pyrazol-1-yl)pyridines—A versatile system for spin-crossover research

Malcolm A. Halcrow*

School of Chemistry, University of Leeds, Woodhouse Lane, Leeds LS2 9JT, UK

Contents

ARTICLE INFO

Article history:
Received 5 June 2009
Accepted 15 July 2009
Available online 23 July 2009

Keywords:
Tridentate ligands
Synthesis
Iron complexes
Spin-crossover
LIESST

ABSTRACT

Synthetic procedures are available for the derivatisation of almost every position of the 2,6-di(pyrazol-1-yl)pyridine (1-bpp) skeleton. This has led to the preparation of a large number of iron(II) complexes of the $[Fe(1\text{-}bpp)_2]^{2+}$ type, many of which undergo spin-crossover transitions at accessible temperatures, sometimes around room temperature. This review surveys these compounds, and presents a wider discussion of their structural chemistry and photomagnetic properties. The availability of a series of chemically similar spin-transition materials has allowed trends in their behaviour to be identified and correlated with their molecular and lattice structures. This represents a rare, positively identified structure:function relationship for spin-crossover materials. Other topics under discussion are the existence of a novel angular Jahn–Teller distortion in several of these compounds and its consequences for spin-crossover; and, the normal and abnormal behaviour of different $[Fe(1\text{-}bpp)_2]^{2+}$ materials trapped in metastable high-spin states at low temperature.

1. Introduction

Several classes of transition metal compound can adopt either a high- or low-spin electronic state, containing the highest or lowest possible number of unpaired electrons. If the energy difference between the two configurations is small, a “spin-crossover” transition between the two can be induced by an external stimulus

* Fax: +44 113 343 6565.
E-mail address: M.A.Halcrow@leeds.ac.uk.

0010-8545/$ – see front matter © 2009 Elsevier B.V. All rights reserved.
doi:10.1016/j.ccr.2009.07.009

[1–3]. Most commonly these transitions are induced by a change in temperature, but they can also be achieved by irradiation [2–4], by application of pressure [5], or in an applied magnetic field. The phenomenon is most common in octahedral iron(II) [6], iron(III) [7] and cobalt(II) [8] complexes, but several other combinations of metal ion and coordination geometry can also give rise to the effect [9].

A thermal spin transition in a spin-transition molecule results in changes to several of its physical properties [10], including its magnetic moment, colour, molecular structure [11], dielectric constant [12] and electrical resistance [13]. Functional liquid crystals and Langmuir–Blodgett films [14,15], nanoparticles [16], thin films and surface patterns [13,17] of spin-transition materials have also been demonstrated, whose functionality is comparable to that of the corresponding bulk materials. These properties have led to several applications of spin-transition materials, including: a display device with pixels of a spin-transition material whose colour is switched by spot-heating and cooling [18]; an electroluminescent device, where a thin film of a spin-transition compound quenches light-emission through changes in its electrical resistance [19]; and, a temperature-sensitive MRI contrast agent [20]. On a still smaller scale, spin-crossover can be used to modulate other physical phenomena at the molecular level [21]. The greatest success has been achieved with double salts of spin-transition cations and potentially conducting metal/dithiolene anions [22,23], where contraction of the cation sub-lattice can cause a change in the conductivity at the spin-transition temperature [23]. Because of these applications, there is still great interest in understanding the solid-state chemistry and physics of spin-state transformations, so that switchable materials with predictable bulk properties can be *designed*. Whether a transition occurs gradually or abruptly, continuously or discontinuously with decreasing temperature, and if it exhibits hysteresis, are determined by the dimensionality and strength of inter-molecular interactions in the bulk solid [24]. Therefore, the study of spin transitions is largely a question of crystal engineering.

In a related phenomenon, low-spin iron(II) compounds may be excited to a metastable high-spin state by irradiation with green or red laser light, which can often have a lifetime of hours below 50 K. This is known as light-induced excited spin-state trapping, or the 'LIESST' effect [2–4]. Below a critical temperature (T_{LIESST}), which can be as high as 130 K [25], the excited state can only relax back to its low-spin ground state by quantum mechanical tunnelling [26]. This can be slow in iron(II) compounds, which often show the largest differences in molecular structure between the high- and low-spin states. Since LIESST compounds are effectively photo-activated molecular switches, there is great interest in finding new compounds with high operating temperatures (that is, in maximising T_{LIESST}) [4].

Although they were discovered relatively recently in the timeframe of spin-crossover research [27], iron(II) complexes of 2,6-di(pyrazol-1-yl)pyridine (1-bpp) and its derivatives have proven to be very flexible compounds for the study of spin transitions (Scheme 1). Synthetic routes have been developed for the functionalisation of almost every site of the 1-bpp skeleton. Substitution at the distal pyrazole 3-positions can modify the steric environment of the coordinated iron ion, giving some control over its spin state [28] (Scheme 1A). Alternatively, substitution at the ligand pyrazole 4-position or pyridine 4-position allows modification of the periphery of the complex, without perturbing the iron centre to a great extent (Scheme 1B and C). Complexes of all the types shown in Scheme 1 often undergo thermal spin-crossover at accessible temperatures, and no other ligand system used in spin-crossover research is so synthetically flexible.

A general review of the syntheses and coordination chemistry of 1-bpp, its regioisomer 2,6-di(pyrazol-3-yl)pyridine (3-bpp, Scheme 1), and their derivatives was published in 2005 [29]. This

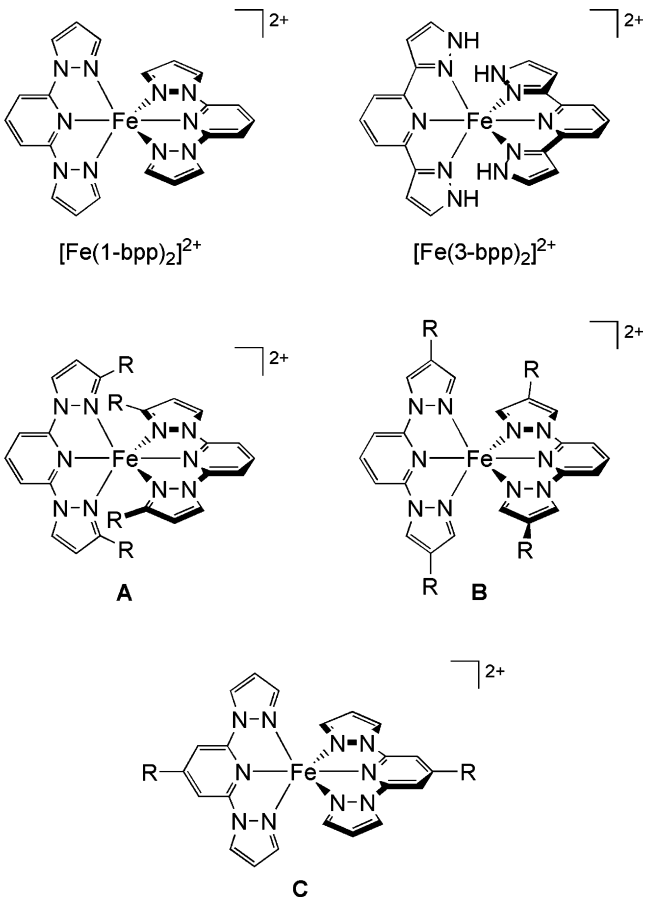

Scheme 1. Structures of $[Fe(1\text{-bpp})_2]^{2+}$ and $[Fe(3\text{-bpp})_2]^{2+}$, and the orientation of ligand substituents at the pyrazole 3-position (A), the pyrazole 4-position (B) and the pyridine 4-position (C) in $[Fe(1\text{-bpp})_2]^{2+}$.

article concentrates on more recent results in the iron chemistry of 1-bpp derivatives, from our laboratory and from other groups. The structural, magnetic and photomagnetic properties of all these compounds are surveyed, to highlight the particular ways in which 1-bpp complexes have contributed to our understanding of spin-crossover chemistry.

2. Complexes of 2,6-di(pyrazol-1-yl)pyridine (1-bpp)

2.1. $[Fe(1\text{-bpp})_2][BF_4]_2$

The prototype compound in the series is $[Fe(1\text{-bpp})_2][BF_4]_2$, which undergoes an abrupt and complete thermal spin transition centred at 260 K (Fig. 1) [27,30]. This transition exhibits a narrow but reproducible hysteresis loop, 3 K in width. The same solvent-free crystal phase of the compound is obtained at room temperature from all common organic solvent mixtures, in the monoclinic space group $P2_1$ [27,31,32]. Single crystal structures above and below the transition temperature confirm that there is no change in crystallographic symmetry during spin-crossover, nor does there appear to be a change in the extensive BF_4^- anion disorder at these temperatures (anion ordering does occur on cooling, but only at a temperature between 150 and 240 K) [27]. Interestingly, the enthalpy of spin-crossover in solid $[Fe(1\text{-bpp})_2][BF_4]_2$ from DSC measurements varies significantly, between samples crystallised from acetone/Et_2O (16.6 kJ mol^{-1}) [27], MeCN/Et_2O (17.2 kJ mol^{-1}) [31] and $MeNO_2$/Et_2O (21.8 kJ mol^{-1}) [32]. The single crystal structures, phase purity (by X-ray powder diffraction) and the form of the spin transitions (from magnetic susceptibility data) are the same in

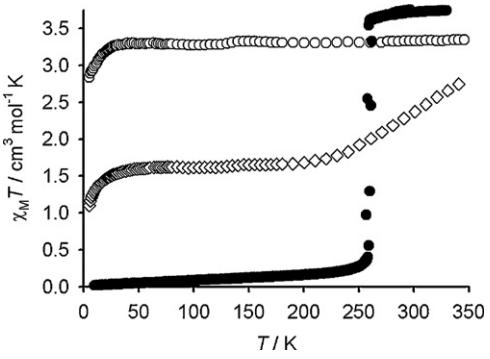

Fig. 1. Variable temperature magnetic susceptibility data for three salts of [Fe(1-bpp)$_2$]X$_2$: X$^-$ = BF$_4^-$ (●) [27,30], X$^-$ = [Co(C$_2$B$_9$H$_{11}$)$_2$]$^-$ (◊) [39] and X$^-$ = PF$_6^-$ (○) [30]. Data for the BF$_4^-$ salt were measured in both cooling and warming mode.

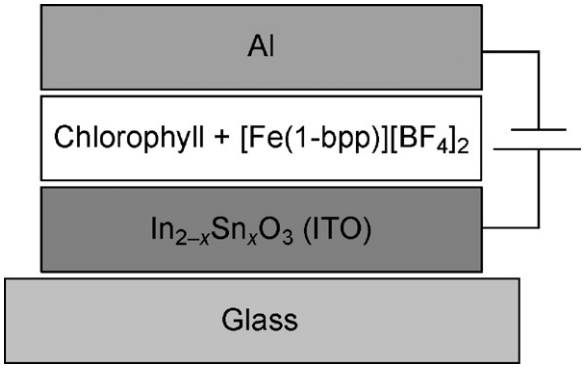

Scheme 2. Design of a temperature-dependent electroluminescence device based on a spin-coated thin film of [Fe(1-bpp)$_2$][BF$_4$]$_2$ and chlorophyll [19].

all three samples. It was suggested that the solvent-dependent thermodynamics of spin-crossover in [Fe(1-bpp)$_2$][BF$_4$]$_2$ might reflect the different crystal morphologies obtained from these solvents [32]. While small, well-formed single crystals are obtained upon diffusion of Et$_2$O into acetone and MeCN solutions of the compound, crystallisation from MeNO$_2$/Et$_2$O affords large blocks of aggregated material. The LIESST effect shown by [Fe(1-bpp)$_2$][BF$_4$]$_2$ is described in Section 8 below [33–35].

Crystallisation of [Fe(1-bpp)$_2$][BF$_4$]$_2$ from MeNO$_2$/Et$_2$O at 240 K (below the spin-transition temperature) affords a different, solvated phase of the material, of approximate formula [Fe(1-bpp)$_2$][BF$_4$]$_2$·3CH$_3$NO$_2$ [30]. This phase contains two unique complex cations in its asymmetric unit, both of which are low-spin, and is only stable below about 260 K. Above that temperature the dark brown crystals decompose spontaneously to a yellow powder, the change in colour indicating a concomitant transition to a high-spin state. For two different phases of a compound to undergo spin-crossover abruptly at (essentially) the same temperature is extremely unusual. An analogous recrystallisation of [Fe(1-bpp)$_2$][BF$_4$]$_2$ from MeCN/Et$_2$O at 240 K instead affords the same solvent-free material that is obtained at room temperature [30].

Three theoretical studies of [Fe(1-bpp)$_2$][BF$_4$]$_2$ have been reported. A combined crystal field/molecular mechanics calculation of both spin states of the cation reproduced their molecular geometries accurately, and correctly predicted its low-spin ground state at 0 K [36]. A static density functional (DF) calculation reached the same conclusion [30]. However a recent, more detailed DF study has mapped out the complete low → high and high → low-spin conversion pathways in [Fe(1-bpp)$_2$]$^{2+}$, and analysed the electronic states involved [37]. The distortion of the molecule from an ideal octahedral geometry, caused by the narrow ligand bite angle, has the effect of allowing singlet ↔ quintet interconversion *via* intermediate triplet states. These are not accessible in a perfectly octahedral iron(II) complex, which can only undergo spin-crossover directly through a double intersystem crossing [37].

Smooth thin films of [Fe(1-bpp)$_2$][BF$_4$]$_2$ of 30 nm thickness can be spin-coated onto a glass substrate from MeCN solution [13]. These films also undergo spin-crossover at 260 K, albeit with a slightly reduced cooperativity (the thermal transition width is around 15 K) and only to around 75% completeness. The 25% residual high-spin fraction at low temperatures may reflect an increased number of lattice defects in the thin film, or the film's relatively high surface area (since molecules outside the bulk of the material may be inactive). The electrical resistance of the film decreases by 25% across the spin transition [13], which has been utilised in the preparation of an electroluminescent device (Scheme 2). The lower resistance of the low-spin state makes it less efficient at transferring charge carriers to the luminescent chlorophyll centres, which quenches the luminescence below 260 K [19].

Evans method measurements showed that [Fe(1-bpp)$_2$][BF$_4$]$_2$ also undergoes spin-crossover in solution, with $T_{½}$ = 248 K in d^6-acetone [30]. The enthalpy of the transition derived from these data, ΔH = 24.1 kJ mol^{-1}, is slightly higher than in the solid state (see above) but is still within the range usually found for spin-crossover compounds. That implies the compound does not undergo significant solvolysis under these conditions [38].

2.2. Other salts of [Fe(1-bpp)$_2$]$^{2+}$

Despite the behaviour of the BF$_4^-$ salt, only one other salt of this cation exhibits a thermal spin transition. That is [Fe(1-bpp)$_2$][Co(C$_2$B$_9$H$_{11}$)$_2$]$_2$, which forms nitromethane solvate crystals containing two unique molecules per asymmetric unit (Fig. 2) [39]. The magnetic moment of the dried material decreases gradually upon cooling, from $\chi_M T$ = 2.7 cm^3 mol^{-1} K at 340 K to a plateau of 1.7 cm^3 mol^{-1} K at 220 K and below (Fig. 1). That implies that 50% of the iron sites in the material undergo a gradual spin transition, whose midpoint is approximately 318 K, while the other 50% remain high-spin at low temperatures. That is consistent with the crystallographic analysis, in which one of the two crystallographically unique cations (molecule "A") is clearly low-spin at 150 K but partially high-spin at 300 K, from its Fe–N bond lengths at each temperature. In contrast the other molecule "B" has bond lengths that are the same at both temperatures, and imply it is high-spin. Notably, the high-spin molecule B has a coordination geometry that is noticeably distorted, compared to molecule A. This is evident in the *trans*-N{pyridine}–Fe–N{pyridine} angle, which is 178.3(3)° for molecule A and 159.6(3)° in molecule B at 150 K (Fig. 2) [39]. This angle would be 180° in a [Fe(1-bpp)$_2$]$^{2+}$ cation with the highest possible D_{2d} symmetry.

Five other [Fe(1-bpp)$_2$]X$_2$ salts have been reported, with X$^-$ = PF$_6^-$ [30], ClO$_4^-$, SbF$_6^-$ [40] and I$_3^-$ [41], plus a mixed iodide/triiodide salt [Fe(1-bpp)$_2$]I$_{0.5}$[I$_3$]$_{1.5}$ [39]. All five compounds form solvent-free crystals that are fully high-spin between 5 and 300 K (Fig. 1); the PF$_6^-$, ClO$_4^-$ and SbF$_6^-$ salts are isostructural. They each adopt the distorted coordination geometry shown by molecule B in Fig. 2, often with even stronger deviations from regularity. The occurrence of this unusual coordination geometry, and its influence on the spin-crossover behaviour, is discussed in more detail in Section 5.

3. Derivatives of 1-bpp substituted at the pyrazole ring

3.1. Ligand syntheses

Derivatisation of the pyrazole rings of the 1-bpp framework is most readily achieved by reacting 2,6-dibromopyridine with the sodium or potassium salt of the preformed substituted pyrazole in

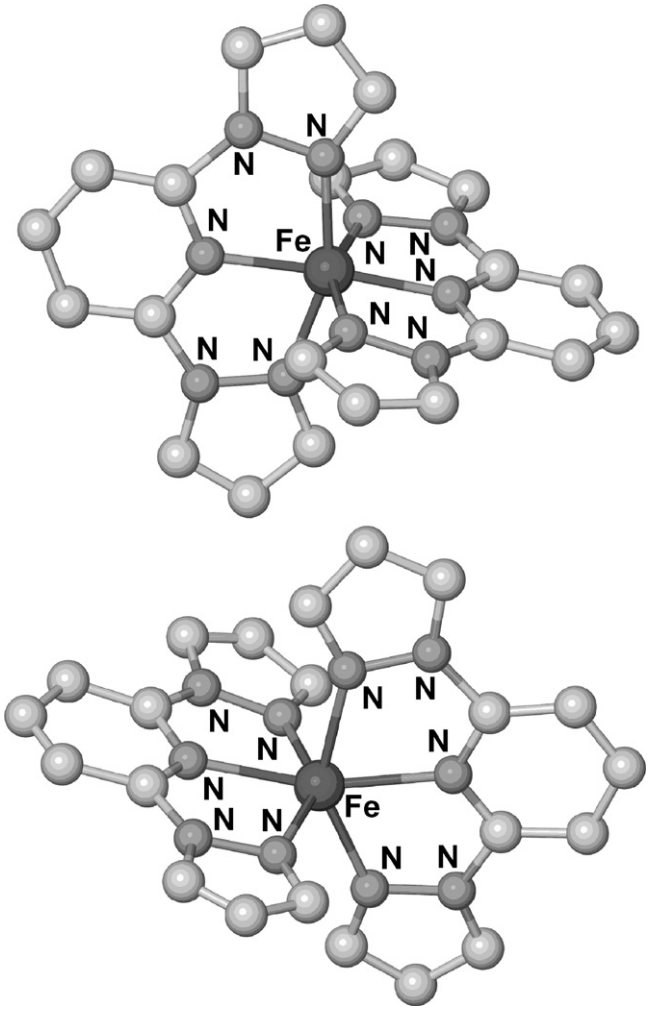

Fig. 2. Comparison of the structures of molecule A (top) and molecule B (bottom) in $[Fe(1\text{-bpp})_2][Co(C_2B_9H_{11})_2]_2$ [39].

hot diglyme, Eq. (1) [42].

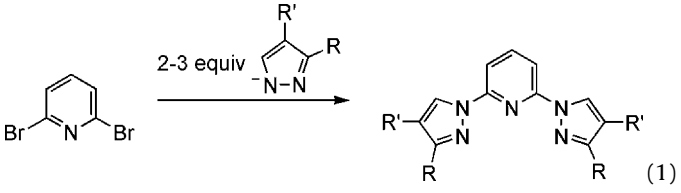

(1)

The reaction is slow, usually requiring 4–5 days to complete, and gives 40–70% yield of purified product depending on the pyrazole used. The most common impurities are the monosubstituted intermediate **I** [42] and, where an unsymmetrically substituted pyrazole is used, the more sterically hindered regioisomer **II** (Scheme 3) [39,42,43]. Contamination by **I** is often minimised, by using excess pyrazole during the reaction. The reaction time can be reduced by palladium catalysis, although this does not result in increased yields or product selectivity [44]. Variation of the reaction conditions allows the two substitution steps to occur separately in two steps, yielding unsymmetric derivatives **III** (Scheme 3) [42].

Most 1-bpp derivatives that have been made in this way contain 3-substituted pyrazolyl groups (Eq. (1); R = alkyl, aryl or carboxy; R′ = H), since the corresponding 3{5}-substituted-1*H*-pyrazole precursors are often commercially available or are easily prepared on a large scale from cheap starting materials [45] (Scheme 4).

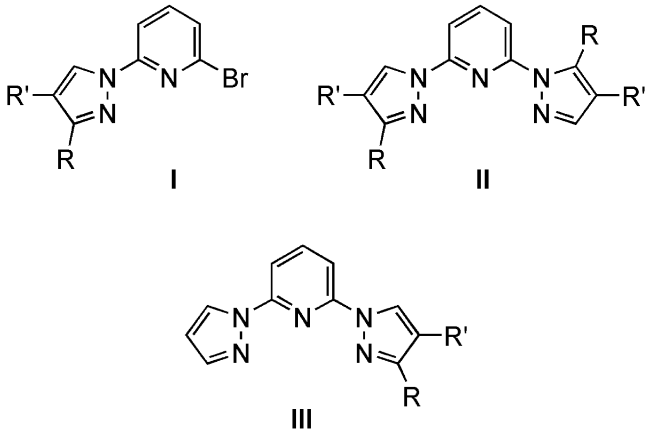

Scheme 3. Common byproducts and unsymmetric derivatives from Eq. (1).

The synthesis of 4-substituted pyrazoles (Eq. (1); R = H; R′ = alkyl, aryl or carboxy) on a gram scale is more difficult [45]. However two such compounds that are commercially available are 4-methylpyrazole, which yields L^3 when used in Eq. (1), and ethyl pyrazole-4-carboxylate which is converted to L^{10} (Scheme 4).

Preformed 1-bpp can be halogenated at the pyrazole 4-positions using electrophilic reagents, yielding the dichloro, dibromo and diiodo derivatives in Scheme 5 [52,53]. Attempted nitration of 1-bpp with HNO_3/H_2SO_4 yields a mixture of compounds, however, through partial nitration of the pyridine as well as the pyrazole rings [54]. 2,6-Di(4-iodopyrazol-1-yl)pyridine (L^{18}) can be coupled with alkynes under Sonogashira conditions [53,55], and converted to a Grignard reagent for quenching with electrophiles [53]. The latter method has used to make 2,6-di(pyrazol-1-yl)pyridine-4′,4″-dicarbaldehyde, a useful synthon for further derivatisation [53]. None of these products have yet been used to make metal complexes, however. Reduction of the diesters L^{10} and L^{11} yields the corresponding di(hydroxymethyl) derivatives L^{18} and L^{19} in moderate yields [48,49] (Scheme 5).

3.2. Complexes of 3′,3″-disubstituted ligands

Substituents at the pyrazole 3-positions exert an electronic and steric influence on the coordinated metal ion. Electronically, substituents adjacent to the pyrazole *N2* donor atoms have an inductive influence on their basicity, as can be seen in basic pK_a values of the corresponding *N*H pyrazoles [56]. Sterically, the disposition of the two ligands in a D_{2d}-symmetric $[ML_2]^{2+}$ complex means the pyrazole substituents of each ligand sandwich the pyridyl ring of the other, at a distance of only 3.3–3.5 Å to the geminal substituent carbon atoms (Fig. 3). Despite these considerations, the $[Fe(1\text{-bpp})_2]^{2+}$ moiety is sterically flexible enough to accommodate a range of distal substituents. Only L^6, of the ligands in Schemes 4 and 5, is too hindered to form a $[Fe(L^6)_2]^{2+}$ complex with iron(II); treatment of $Fe[BF_4]_2{\cdot}6H_2O$ with 2 equiv. of that ligand in acetone instead yields crystals of $[Fe(L^6)(OH_2)_2(O{=}C\{CH_3\}_2)][BF_4]_2$ [57].

These considerations are exemplified by comparison of $[Fe(L^5)_2]^{2+}$ and $[Fe(L^8)_2]^{2+}$ (Scheme 4), whose electron-donating *iso*propyl and mesityl groups might both be expected to stabilise the low-spin form of the compounds. However, salts of $[Fe(L^5)_2]^{2+}$ are high-spin at room temperature and below, in solution and the solid state, which is attributed to steric repulsions between the two ligands preventing the contraction of the Fe–N bonds required for the low-spin state (Fig. 3, top) [28,40]. In contrast $[Fe(L^8)_2]^{2+}$ is low-spin as expected, because its flat mesityl substituents do not exert the same steric influence when co-parallel to the plane of the other ligand (Fig. 3, bottom) [28,58]. The least squares planes of the sand-

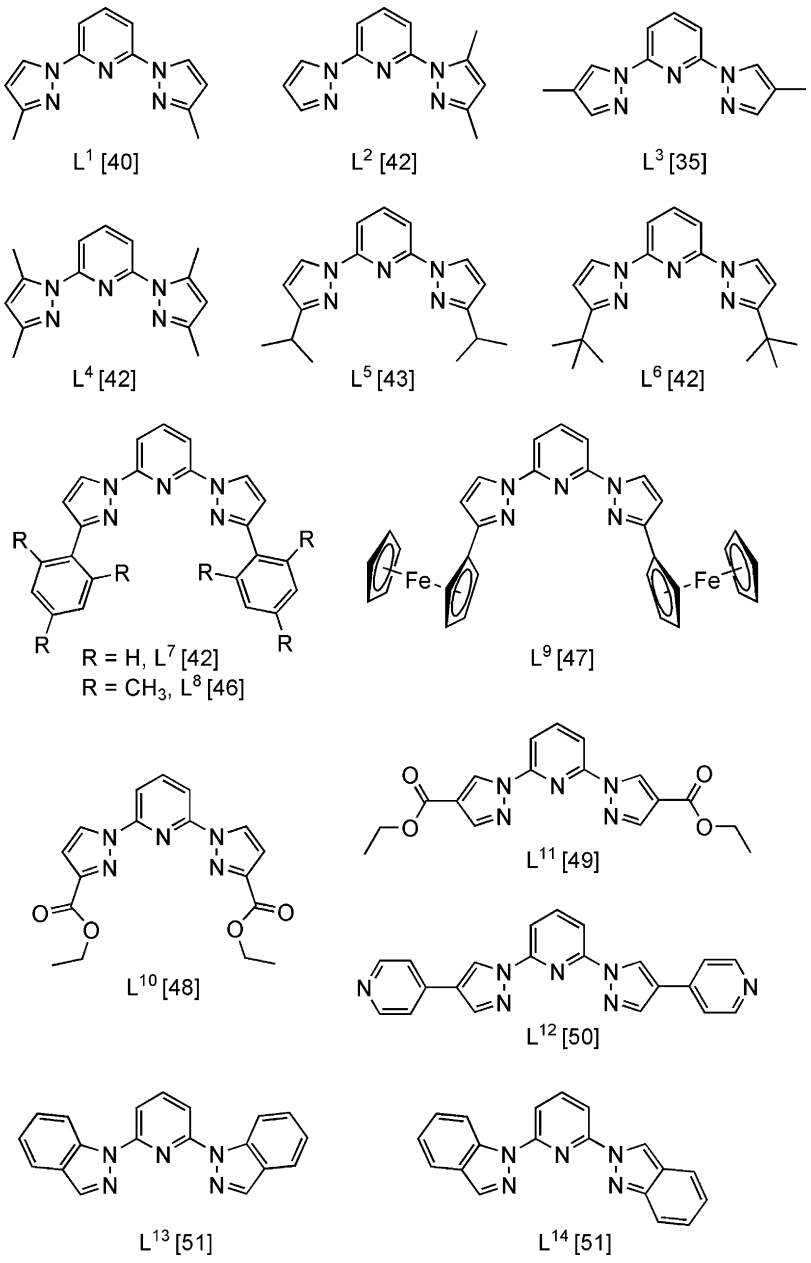

Scheme 4. Derivatives of 1-bpp substituted at the pyrazole ring, synthesised by Eq. (1), that have been used to make iron(II) complexes. References are for the syntheses of the ligands.

wiched pyridyl and mesityl groups in $[Fe(L^8)_2]^{2+}$ are within 4.0° of coplanarity and are 3.318(7)–3.387(7) Å apart, essentially equal to the sum of covalent radii of two aromatic rings. The compounds $[Fe(L^7)_2][BF_4]_2$ [28,40], $[Fe(L^9)_2][BF_4]_2$ [47] and $[Fe(L^{10})_2][BF_4]_2$ [40] are all high-spin in the solid state and, where measured, in solution. Since the L^7 and L^9 complexes are sterically comparable to $[Fe(L^8)_2]^{2+}$, that must reflect stabilisation of the high-spin state by their electron-withdrawing phenyl and ferrocenyl substituents [28].

The ligands L^1 and L^{18} (Schemes 3 and 4), whose distal substituents are small, do form spin-crossover complexes with iron(II). The three known salts of $[Fe(L^1)_2]^{2+}$ show particularly varied behaviour. Crystals of the BF_4^- salt grown from MeOH/Et_2O have the formula $[Fe(L^1)_2][BF_4]_2{\cdot}xH_2O$ [59]. In freshly prepared material $x \approx 1/3$, but the lattice water is lost under ambient conditions over a period of weeks, without affecting the crystallinity of the sample. Both single crystals and bulk material undergo an abrupt spin transition to *ca.* 50% completeness. In single crystals, the temperature of this transition is different in the presence ($90 < T_{½} < 130$ K) or absence ($150 < T_{½} < 160$ K) of the lattice water. Bulk samples of the compound are usually partially dehydrated and exhibit both features at $T_{½} = 105$ and 147 K, each with thermal hysteresis (Fig. 4). The low-temperature phase (*C*2/*c*, *Z* = 24) adopts the same space group as the high-spin material (*C*2/*c*, *Z* = 8), but with a tripled asymmetric unit. Of the three unique cation sites in this mixed-spin phase, one is high-spin and one is low-spin, while the third contains a mixture of the two [59]. Fully low-spin $[Fe(L^1)_2][BF_4]_2{\cdot}xH_2O$ can be obtained by poising the sample at 100 K for 1.5 h (Fig. 4), and is now isostructural with the fully high-spin compound (*C*2/*c*, *Z* = 8). Hence thermal spin-crossover proceeds in two steps (high-spin ↔ mixed-spin and mixed-spin ↔ low-spin), with the second step being kinetically slow [59]. Spin-crossover proceeding through an intermediate phase [60,61], and slow spin-transition kinetics at temperatures below 100 K [62], are both rare phenomena. The

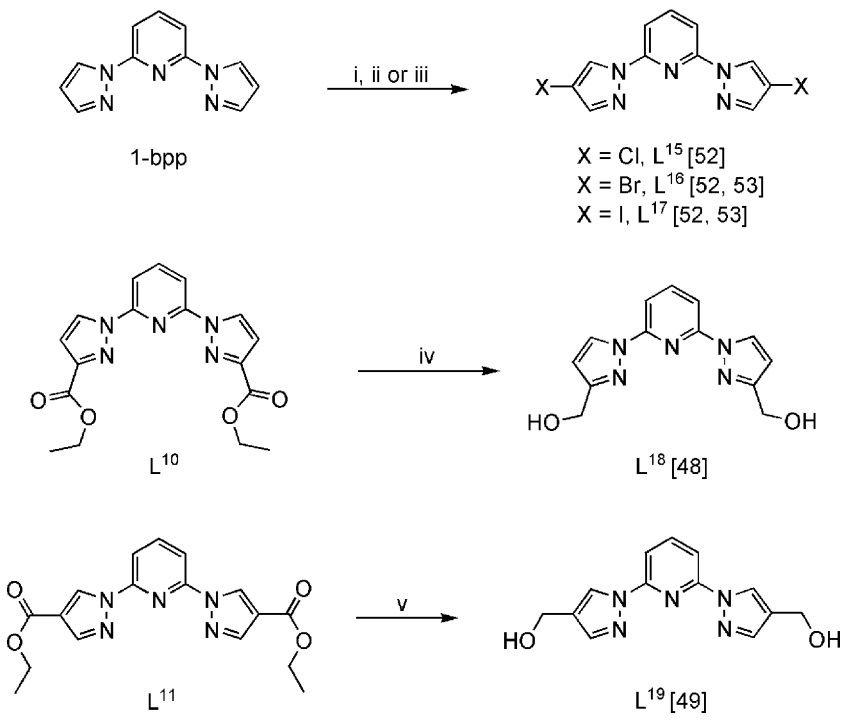

Scheme 5. Synthetic modification of the pyrazole rings in preformed 1-bpp derivatives. Reagents and conditions: (i) NaClO, CH_3CO_2H/H_2O, rt, 2 h. (ii) Br_2, CH_3CO_2H, rt, 5 h. (iii) I_2, $[NH_4]_2[Ce(NO_3)_6]$, CH_3CN, 50 °C, 21 h then rt, 36 h or I_2, HIO_3, CH_3CO_2H, 70 °C, 1 h. (iv) $LiAlH_4$, thf, rt, 3 h. (v) $NaBH_4$, thf, 70 °C, 2 h.

LIESST properties of this material are also very unusual, and are discussed in Section 8.

In contrast, $[Fe(L^1)_2][ClO_4]_2$ (which is not isostructural with the BF_4^- salt) undergoes a very gradual thermal spin transition, centred near 265 K but spanning a temperature range of over 200 K [63]. Two solvated phases $[Fe(L^1)_2][BF_4]_2{\cdot}4CH_3CN$ and $[Fe(L^1)_2][ClO_4]_2{\cdot}(CH_3)_2CO$ have also been isolated, and show similarly gradual spin-crossover with $T_{½} \approx 175$ K [39]. Finally $[Fe(L^1)_2][SbF_6]_2$ is high-spin between 5 and 300 K, despite having a near-regular iron coordination geometry (Sections 2.2 and 5). This is attributed to an increased conformational rigidity caused by a particularly twisted L^1 ligand conformation, that results from a short intermolecular steric contact between pyrazole groups on neighbouring molecules [39].

The unsolvated BF_4^- and ClO_4^- salts of $[Fe(L^{18})_2]^{2+}$ are both high-spin (Section 5) [40,64]. However the crystalline solvate $[Fe(L^{18})_2][ClO_4]_2{\cdot}3/4CH_3CN$ does undergo spin-crossover, at a temperature between 100 and 200 K [64]. Although only crystallographic characterisation of this transition was possible, it is clear that the iron sites in the crystal are all high-spin at 200 K, and but have close to a 1:1 high:low-spin population at 100 K. The crystal packing in this compound implies that the transition cannot proceed to more than 50% completeness. A steric clash between hydroxymethyl groups of two adjacent cations, when both are low-spin, suggests that no more than one molecule in each pair can adopt a low-spin state at low temperatures [64].

3.3. Complexes of 4′,4″-disubstituted ligands

Two polymorphs of $[Fe(L^{15})_2][BF_4]_2$ have been isolated (Scheme 5) [52]. The major 'α' polymorph is isostructural with $[Fe(L^3)_2][ClO_4]_2$ [35] and $[Fe(L^{16})_2][BF_4]_2$ [65] at room temperature, in the tetragonal space group $P\bar{4}2_1c$, and all three compounds undergo abrupt spin transitions that are very similar in form to that shown by $[Fe(1\text{-bpp})_2][BF_4]_2$ [35,52]. The temperatures of these transitions are $T_{½} = 233$ (L = L^3), 202 (L = L^{15}) and 253 K (L = L^{16}). Differential scanning calorimetry (DSC) data showed that the transition temperatures in $[Fe(L^{15})_2][BF_4]_2$ and $[Fe(L^{16})_2][BF_4]_2$ reflect a higher transition enthalpy in the L^{16} complex; the transition entropies of the two compounds are identical within experimental error [52]. α-$[Fe(L^{15})_2][BF_4]_2$ transforms to the $P2_1$ space group in its low-spin state, isostructural with $[Fe(1\text{-bpp})_2][BF_4]_2$; $[Fe(L^{16})_2][BF_4]_2$ probably behaves in the same way from powder diffraction data [52,65]. Interestingly, however, while low-spin $[Fe(L^3)_2][ClO_4]_2$ also undergoes a crystallographic phase change during spin-crossover, its low-spin form adopts the different space group $P2_12_12_1$ [35].

The magnetic susceptibility properties of the 'β' polymorph of $[Fe(L^{15})_2][BF_4]_2$ are very different, with $\chi_M T = 1.2\ cm^3\ mol^{-1}\ K$ at 300 K which implies it is only 1/3 high-spin at room temperature. This value decreases gradually on cooling, showing that the high-spin fraction undergoes a gradual spin-crossover centred near 137 K (Fig. 5) [52]. Although crystals of the β form suffer from mild twinning it is clear they contain two unique iron sites, one of which is twice as abundant as the other in the lattice. The majority site is low-spin at 150 K, while the minority site contains a mixture of high- and low-spin molecules at that temperature and is clearly the one undergoing the spin transition. DSC data showed a broad feature at 411 K for β-$[Fe(L^{15})_2][BF_4]_2$ with no concomitant mass loss by thermogravimetric analysis (TGA), which may correspond to spin-crossover of the remaining iron content in the material [52]. Susceptibility and powder diffraction data suggest that $[Fe(L^3)_2][ClO_4]_2$ is also contaminated by a second, minor low-spin polymorph. This may be isostructural with the BF_4^- salt of the same cation, which is low-spin at room temperature [35].

The iodo-substituted complex $[Fe(L^{17})_2][BF_4]_2$ is low-spin at 350 K and below, and exhibits no spin transition below its thermal decomposition temperature by DSC and TGA. It forms low-spin bis-acetone solvate crystals, that are sometimes contaminated by a second mono-acetone solvate that is high-spin at room temperature [52]. $[Fe(L^{11})_2][BF_4]_2{\cdot}2CF_3CH_2OH$ and $[Fe(L^{19})_2][BF_4]_2{\cdot}H_2O$ (Scheme 5) both exhibit $\chi_M T = 0.3\ cm^3\ mol^{-1}\ K$ at 300 K [49]. For the L^{11} complex this does not vary between 50 and 300 K, implying that it exists as a low-spin compound that is contaminated by

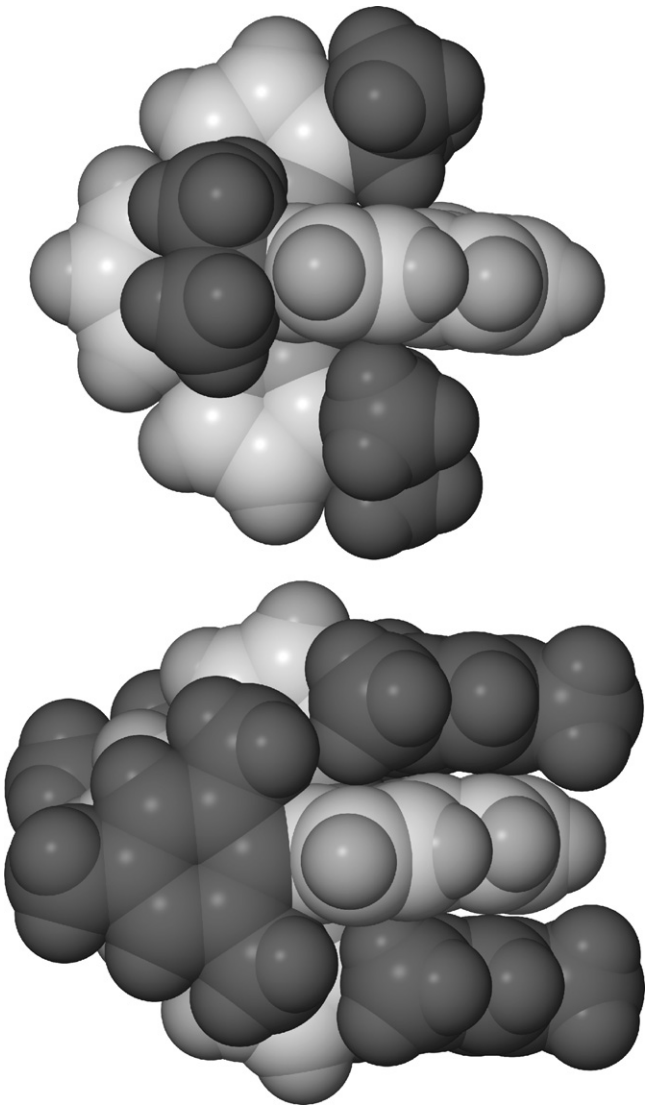

Fig. 3. Crystallographic space-filling models of high-spin $[Fe(L^5)_2]^{2+}$ (top) and low-spin $[Fe(L^8)_2]^{2+}$ (bottom), showing the steric interactions between the distal substituents on one ligand and the pyridyl ring of the other [28,40]. The *iso*propyl and mesityl ligand subsituents are highlighted for clarity.

around 10% of a second high-spin polymorph. The majority low-spin crystal form was structurally characterised. However, cooling $[Fe(L^{19})_2][BF_4]_2{\cdot}H_2O$ does gradually decrease its magnetic moment, to effectively zero below 200 K. Therefore, this compound appears to undergo a gradual thermal spin transition centred above room temperature, that is accompanied by loss of the lattice water by DSC and TGA [49]. Salts of $[Fe(L^{12})_2]^{2+}$ are poorly crystalline and high-spin at room temperature, but undergo extremely gradual and incomplete spin transitions upon cooling [50].

Solution phase spin-crossover equilibria have been measured for most of the compounds in this Section, and are all centred below room temperature (Table 1). The ΔH values in Table 1 are all very similar, and again imply that the complexes retain their molecular structures in these solvents [38]. Hence, the data in Table 1 are a true reflection of the spin states of the compounds, in the absence of any crystal packing effects. It is therefore noteworthy that, although the differences are small, the $T_{½}$ values exactly follow the ordering expected from the inductive properties of the pyrazole group substitutents.

$$L^3 > L^{19} > 1\text{-bpp} \approx L^{11} > L^{16} > L^{15}$$

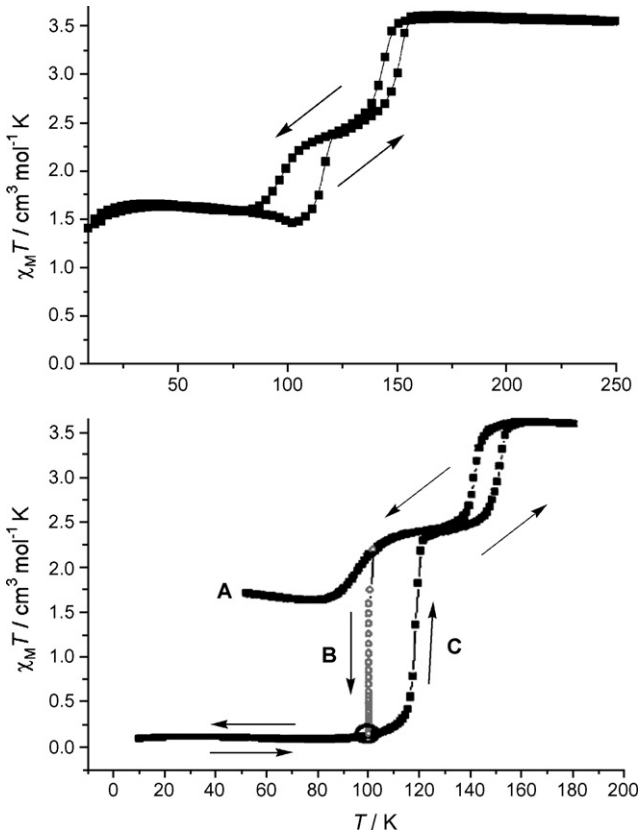

Fig. 4. Variable temperature magnetic susceptibility data for $[Fe(L^1)_2][BF_4]_2{\cdot}xH_2O$ [59]. Top: thermal cycling at 1 K min^{-1}, showing the high-spin → mixed-spin transition. The features centred at 105 and 147 K originate from hydrated and dehydrated parts of the sample. Bottom: A, cooling through the high-spin → mixed-spin transition; B, the sample is annealed at 100 K for 90 min, causing the susceptibility to decrease as shown as the mixed-spin → low-spin transition takes place; C, the sample is cooled further to 5 K then rewarmed, showing the reversibility of the process.

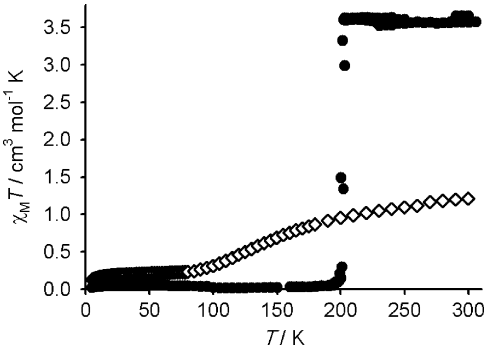

Fig. 5. Variable temperature magnetic susceptibility data for the α (●) and β (◊) polymorphs of $[Fe(L^{15})_2][BF_4]_2$ [52]. Data for the α form were measured in both cooling and warming mode.

Table 1
Solution-phase spin-crossover data for $[FeL_2][BF_4]_2$ complexes, where L is 1-bpp or a derivative substituted at the pyrazole 4-positions (Schemes 4 and 5).

L	Solvent	$T_{½}$ (K)	ΔH (kJ mol^{-1})	ΔS (J mol^{-1} K^{-1})	Reference
1-bpp	$(CD_3)_2CO$	248 (1)	24.1 (2)	101 (1)	[30]
L^3	CD_3NO_2	273 (1)	26.4 (2)	96 (1)	[35]
L^{11}	$(CD_3)_2CO$	246 (1)	24.4 (3)	99 (1)	[49]
L^{15}[a]	CD_3NO_2	231 (2)	–	–	[52]
L^{16}[a]	CD_3NO_2	238 (2)	–	–	[52]
L^{19}	$(CD_3)_2CO$	259 (2)	25.7 (4)	99 (2)	[49]

[a] $T_{½}$ estimated from extrapolation of data below 244 K, the freezing point of the solvent. Not enough of the transition was observed in the liquid range of the solvent to determine ΔH and ΔS accurately.

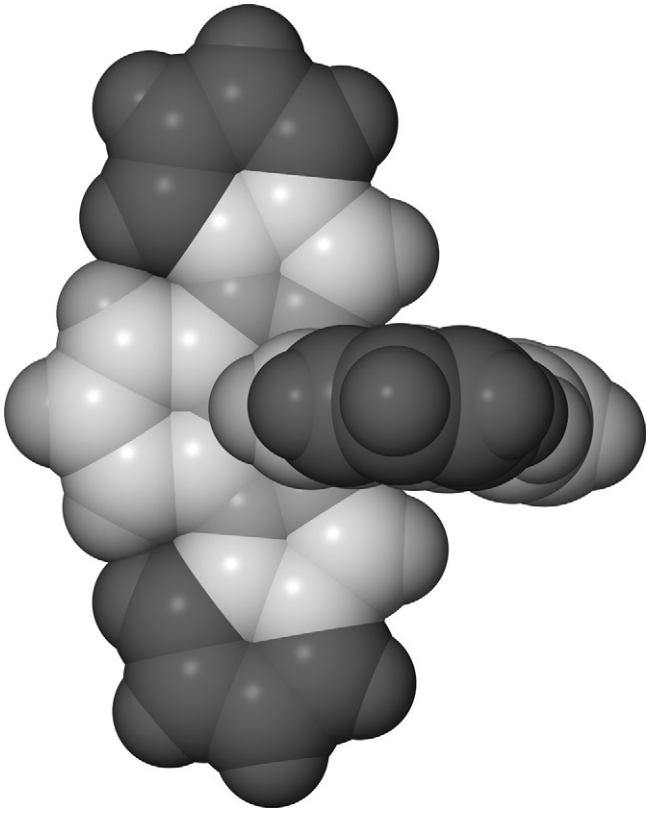

Fig. 6. Crystallographic space-filling model of low-spin $[Fe(L^{13})_2]^{2+}$, showing the intra-ligand steric interactions between the indazole *H*7 and pyridyl *H*3 and *H*5 atoms [51]. The indazole annelated rings are highlighted for clarity.

3.4. Complexes of ligands with other pyrazole substitution patterns

Substitution at the pyrazole 5-positions of a $[Fe(1\text{-bpp})_2]^{2+}$ complex, as in $[FeL_2]^{2+}$ (L = L^2 [29], L^4 [55], L^{13} and L^{14} [51]), results in an intra-ligand steric clash between these substituents and the pyridyl *H*3 and *H*5 atoms (Fig. 6). This promotes the low-spin states of the compounds, by disfavouring the longer Fe–N bonds required in the high-spin state. Hence all four of the complexes listed above are low-spin in the solid state at room temperature [29,51,55], although $[Fe(L^{13})_2][BF_4]_2$ does show evidence for the onset of a spin transition centred above 400 K from susceptibility measurements [54].

4. Ligands substituted at the pyridine ring

4.1. Ligand syntheses

Syntheses of 1-bpp derivatives by Eq. (1) (Section 3.1) can be low-yielding when 4-substituted 2,6-dibromopyridine precursors are used [66,67]. However, two flexible routes to 4-substituted 1-bpp derivatives have been developed. First is *via* 4-hydroxymethyl-2,6-di(pyrazol-1-yl)pyridine (L^{20}, Scheme 6), which is prepared in six steps from commercially available 2,6-dihydroxy-isonicotinic acid [68]. Swern oxidation of L^{20} yields the aldehyde L^{21} [69], which has been used for Wittig reactions [70] or as a precursor to a nitronyl nitroxide derivative [69] (Scheme 6). Alternatively, bromination of L^{20} with HBr [68] or PPh_3/Br_2 [71] gives L^{24}, whose bromomethyl group can then be substituted by a range of nucleophiles (Scheme 6). Lithiation of L^{24} in the presence of 1,2-dibromoethane leads to an oxidative coupling reaction, affording the back-to-back derivative L^{27} [68].

Table 2
Complexes of 4-substituted-2,6-di(pyrazol-1-yl)pyridine derivatives showing moderately gradual spin transitions (Schemes 6 and 7).

	$T_{½}$ (K)	Hysteresis width (ΔT, K)	Reference
$[Fe(L^{20})_2][BF_4]_2$	271	–	[35,77]
$[Fe(L^{20})_2][ClO_4]_2$	284	–	[35]
$[Fe(L^{23})_2][BF_4]_2$	>340	–	[69]
β-$[Fe(L^{28})_2][BF_4]_2$	272	–	[71]
$[Fe(L^{29})_2][ClO_4]_2$	333	–	[75]
$[Fe(L^{30})_2][ClO_4]_2 \cdot 2CH_3CN$[a]	≈200	–	[75]
$[Fe(L^{32})_2][ClO_4]_2$	277	8	[73]
$[Fe(\mu\text{-}L^{33})]_n[BF_4]_{2n}$	323	10	[74]
$[Fe(L^{34})_2][ClO_4]_2$	281	–	[75]
$[FeH(L^{36})_2]_m[ClO_4]_{3m} \cdot mCH_3OH$	286	2	[72]

[a] Transition only proceeds to 50% completeness on cooling. The compound exhibits an unexplained increase in $\chi_M T$ below 50 K.

The second synthetic pathway towards 4-substituted 1-bpp ligands starts from 4-iodo-2,6-di(pyrazol-1-yl)pyridine (L^{29}, Scheme 7), which is accessible in five steps from the same 2,6-dihydroxy-isonicotinic acid starting material [72]. This has proven to be a useful reagent for cross-coupling reactions under Sonogashira and Suzuki–Miyaura conditions, yielding several 4-alkynyl and 4-aryl 1-bpp derivatives (Scheme 7). This includes another "back-to-back" bis-1-bpp, L^{33} from a Suzuki–Miyaura reaction of 1,4-phenylene-diboronic acid with 2 equiv. of L^{29} [74].

4.2. Complexes of 4-substituted ligands

Several iron(II) complexes containing the ligands in Schemes 6 and 7 undergo rather similar moderately gradual thermal spin transitions, mostly around or slightly above room temperature (Table 2, Fig. 7). Two compounds in the table deserve particular comment. First is $[Fe(\mu\text{-}L^{33})]_n[BF_4]_{2n}$, which is a linear oligomer of at least six $[Fe(1\text{-bpp})_2]^{2+}$ moieties linked by covalent 1,4-phenylene spacers (*i.e.* $n \geq 6$) [74]. The spin transition shown by this compound ($T_{½}$ = 323 K) proceeds to *ca.* 85% completion in cooling mode and exhibits a 10 K hysteresis loop, which is unusual in a spin transition that is not abrupt (Section 6). The residual high-spin fraction at low temperatures may originate from $[Fe(OH_2)_3]^{2+}$ sites, whose presence at the ends of the linear oligomers is implied by IR spectroscopy [74]. Second is $[FeH(L^{36})_2]_m[ClO_4]_{3m} \cdot mCH_3OH$, a crystalline supramolecular linear polymer containing $[Fe(L^{36})_2]^{2+}$ centres linked by bridging protons through N–H···N hydrogen bonding to the pendant pyridyl groups (Fig. 8) [72].

Freshly crystallised $[Fe(L^{22})_2][BF_4]_2 \cdot 2(C_2H_5)_2O$ (space group *Fdd*2) loses one molecule of diethyl ether on exposure to air, yielding a new phase $[Fe(L^{22})_2][BF_4]_2 \cdot (C_2H_5)_2O$ (space group *C*2/*c*) in a single crystal-to-single crystal transformation [70]. This transformation is reversed upon incubating the monoetherate in diethyl ether vapour. The diethetate material, and the unsolvated com-

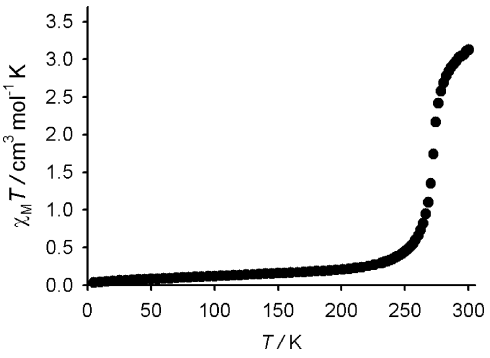

Fig. 7. Variable temperature magnetic susceptibility data for $[Fe(L^{20})_2][BF_4]_2$ [35,77]. Most of the spin transitions listed in Table 2 closely resemble this one, sometimes with the addition of a hysteresis loop.

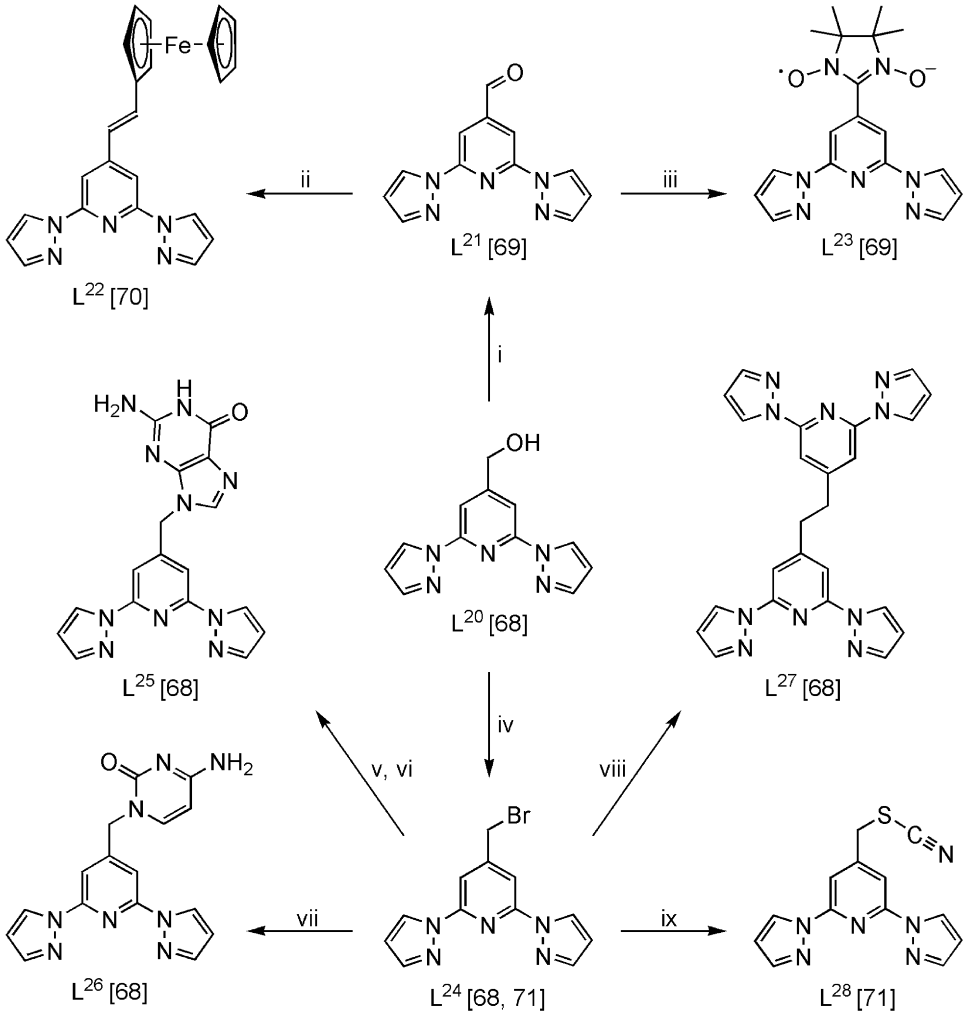

Scheme 6. 4-Substituted 1-bpp derivatives prepared by derivatisation of 4-hydroxymethyl-2,6-di(pyrazol-1-yl)pyridine (L^{20}), that have been used to make iron complexes. Reagents and conditions: (i) $C_2O_2Cl_2$, dmso, CH_2Cl_2, −78 °C, 2 h then NEt_3, rt. (ii) $[FcCH_2PPh_3]I$, KO*t*Bu, thf, reflux, 5 h. (iii) $[(CH_3)_2C(NHOH)]_2$, benzene, rt, 2 weeks then $NaIO_4$, H_2O, rt, 30 min. (iv) 48% HBr, reflux, 4 h or Br_2, PPh_3, CH_3CN, rt, 24 h. (v) Na[9-chloroguaninate], KI (cat), dmf, 50 °C, 5 h. (vi) 0.1 M HCl, reflux, 4 h. (vii) Na[cytosinate], KI (cat), dmf, 50 °C, 5 h. (viii) BuLi, Et_2O, −78 °C then 1,2-$C_2H_4Br_2$, rt, 24 h. (ix) NH_4NCS, CH_3CN, rt, 24 h.

plex, are both high-spin between 5 and 300 K. In contrast, the monooetherate exhibits a gradual spin transition with $T_{½}$ = 230 K [70]. Three other salts of this cation are high-spin at room temperature and below, all of them adopting the unusual distorted coordination geometry that is discussed in Section 5 [78]. The same distorted high-spin molecular structure is also shown by the α polymorph of $[Fe(L^{28})_2][BF_4]_2$ (the other polymorph is a spin-transition phase, Table 2) [71].

The isostructural solvates $[Fe(L^{35})_2]X_2{\cdot}2CH_3CN$ ($X^- = BF_4^-$ and ClO_4^-) both exhibit spin-crossover, but with an unusual dependence on sample history [76]. The freshly prepared materials show gradual, but structured, spin transitions centred at 166 and 179 K, respectively. Both transitions show thermal hysteresis of 6 K ($X^- = BF_4^-$) and 34 K ($X^- = ClO_4^-$) and exhibit a pronounced discontinuity at 30–50% completion. This probably reflects both the onset of a crystallographic phase change, and the existence of more than

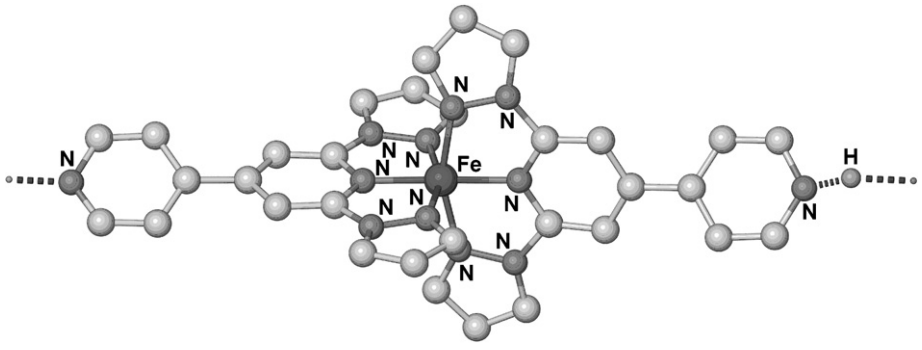

Fig. 8. One complex molecule in the crystal structure of the low-spin form of the supramolecular polymer $[FeH(L^{36})_2]_m[ClO_4]_{3m}{\cdot}mCH_3OH$, showing the association of the cations into chains through N–H···N hydrogen bonding [72].

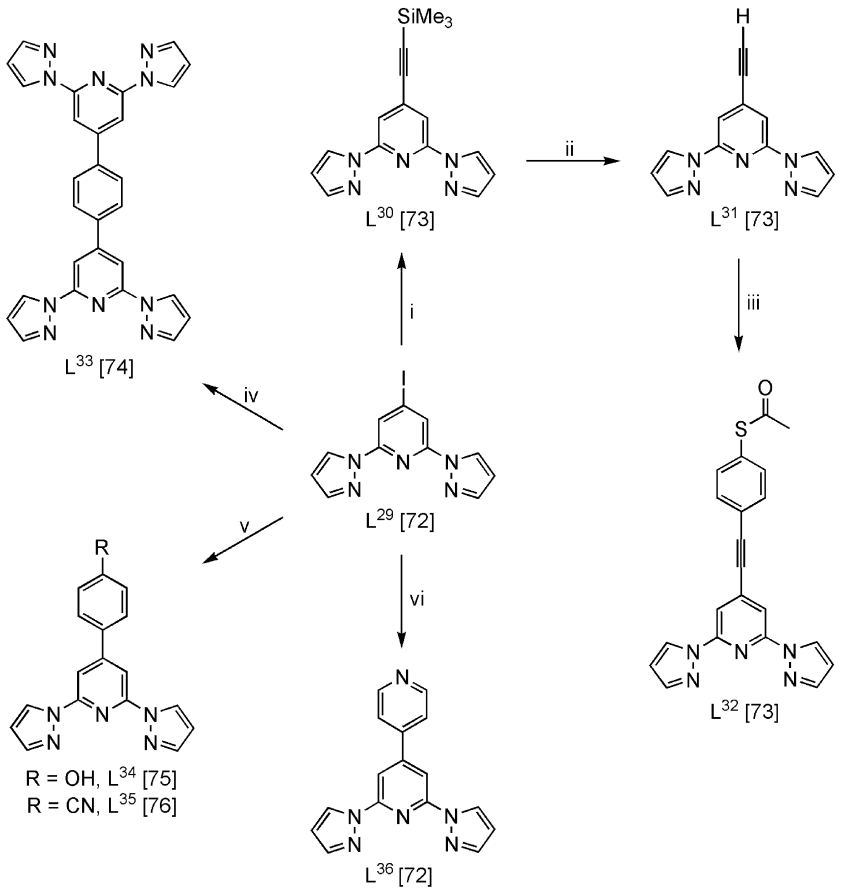

Scheme 7. 4-Substituted 1-bpp derivatives prepared by derivatisation of 4-iodo-2,6-di(pyrazol-1-yl)pyridine (L^{29}), that have been used to make iron complexes. Reagents and conditions: (i) Me_3SiCCH, CuI, $[Pd(PPh_3)_4]$ (cat), N^iPr_2H, thf, 3 days. (ii) K_2CO_3, CH_3OH, CH_2Cl_2, rt, 18 h. (iii) $IC_6H_4SC(O)CH_3$-4, CuI, $[Pd(PPh_3)_2Cl_2]$ (cat), N^iPr_2H, thf, 3 days. (iv) $C_6H_4[B(OH)_2]_2$-1,4, $[Pd(PPh_3)_4]$ (cat), dioxane, Na_2CO_3, 70 °C, 3 days. (v) $RC_6H_4B(OH)_2$-4, $[Pd(PPh_3)_4]$ (cat), CH_3OH, toluene, Na_2CO_3, 70 °C, 2 days. (vi) pyrid-4-ylboronic acid, $[Pd(PPh_3)_4]$ (cat), dioxane, Na_2CO_3, 70 °C, 2 days.

one phase in the powdered samples (a second, minor solvated polymorph was isolated for the BF_4^- salt) [76]. Repeated thermal cycling of the materials causes substantial changes in these data, associated with loss of the acetonitrile solvent. For $[Fe(L^{35})_2][ClO_4]_2$, this leads to collapse of the wide hysteresis loop, but otherwise the spin transition of the desolvated powder retains the discontinuous form of the fresh sample, occurring more obviously in two discrete steps. For the BF_4^- salt, however, the desolvated material behaves very differently, exhibiting a regular spin transition resembling that in Fig. 7, with $T_{½}$ = 236 K. Powder diffraction data for both compounds suggest that crystallographic phase changes occur during desolvation, and that the solvent-free BF_4^- and ClO_4^- salts may not be isostructural [76].

In contrast to the above, salts of $[Fe(L^{25})_2]^{2+}$, $[Fe(L^{26})_2]^{2+}$ and $[Fe(\mu\text{-}L^{27})]_n^{2n+}$ are all high-spin at room temperature, and exhibit extremely gradual spin transitions upon cooling that proceed to no more than 35% completeness [68]. A potential explanation for this poor spin-crossover functionality is given in Section 6. The iron(II) complexes of L^{23} [69], L^{24} [63] and L^{31} [75] are each low-spin in the solid state at room temperature. While the L^{23} complex shows the onset of spin-crossover upon warming to 340 K, the L^{31} complex remains fully low-spin up to 380 K.

Thermal spin-crossover of $[Fe(L^{20})_2][BF_4]_2$ in CD_3NO_2 solution is centred at 281 K, very similar to its $T_{½}$ value in the solid state (Table 2). However, the enthalpy of this process is over twice that for the other compounds in this review (Table 1), at ΔH = 52 kJ mol^{-1} [63]. This higher value suggests that the compound may undergo some ligand dissociation in solution, possibly *via* intermolecular attack of its nucleophilic hydroxyl substituents at the iron centres. $[Fe(L^{28})_2][BF_4]_2$ also undergoes spin-crossover in solution, with a lower $T_{½}$ temperature of *ca.* 215 K [71].

4.3. Complexes of 2,6-di(pyrazol-1-yl)pyrazine and its derivatives

Another way of functionalising 1-bpp is to incorporate additional heteroatoms into its pyridine ring. 2,6-Di(pyrazol-1-yl)pyrazine (L^{37}) is synthesised by Eq. (1) (Section 3.1), employing 2,6-dichloropyrazine as starting material [79], and several of its pyrazole-substituted derivatives have been prepared in the same manner (Scheme 8) [29]. Both salts $[Fe(L^{37})_2]X_2$ ($X^- = BF_4^-$ and ClO_4^-) exhibit abrupt spin transitions that resemble that shown by $[Fe(1\text{-bpp})_2][BF_4]_2$ (Fig. 1), at $T_{½}$ = 219 and 201 K, respectively [80]. High-spin $[Fe(L^{37})_2][ClO_4]_2$ is isostructural with $[Fe(1\text{-bpp})_2][BF_4]_2$ but, unlike the 1-bpp complex, it undergoes a phase change in its low-spin state. Low-spin $[Fe(L^{37})_2][ClO_4]_2$ retains the same space group as the high-spin material ($P2_1$), but with a doubled unit cell *a* axis [81]. Preliminary powder diffraction data imply that high-spin $[Fe(L^{37})_2][BF_4]_2$ is isostructural with the low-spin perchlorate salt, and that it undergoes a further unit cell expansion during its spin transition [80]. A solvate $[Fe(L^{37})_2][BF_4]_2{\cdot}3CH_3NO_2$ was also characterised and undergoes an abrupt spin transition at 198 K, from variable temperature unit cell measurements [80]. This is not isostructural with the *tris*-nitromethane solvate of $[Fe(1\text{-bpp})_2][BF_4]_2$ (Section 2.1) [30].

In contrast to those two salts, $[Fe(L^{37})_2][SbF_6]_2$ is a high-spin compound [82]. The solvent-free crystals are isostructural with

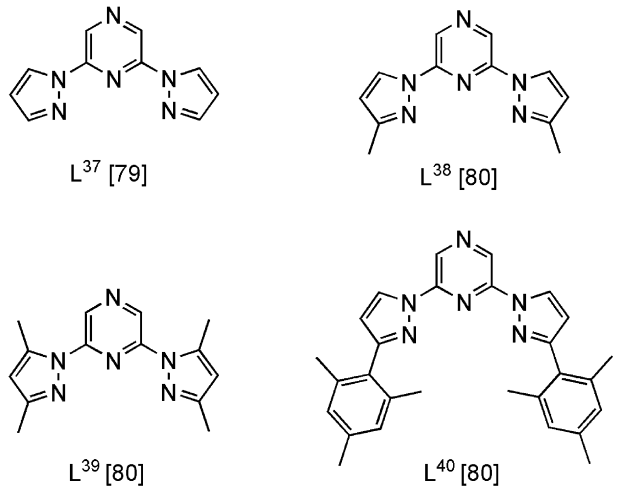

Scheme 8. 2,6-Di(pyrazol-1-yl)pyrazine (L^{37}) and its derivatives substituted at the pyrazole ring, synthesised by Eq. (1), that have been used to make iron(II) complexes.

$[Fe(1\text{-bpp})_2][SbF_6]_2$, and exhibits the same distorted high-spin coordination geometry that is discussed in Section 5. This is the only known example where a complex of a 1-bpp derivative, and its 2,6-di(pyrazol-1-yl)pyrazine analogue, have the same structural chemistry. Two nitromethane solvates of $[Fe(L^{37})_2][SbF_6]_2$ were also crystallised, one high-spin and the other low-spin [82]. Spin-crossover in d^6-acetone solutions of $[Fe(L^{37})_2][SbF_6]_2$ is centred at 268 K, 27 K higher than for $[Fe(1\text{-bpp})_2][BF_4]_2$ (Section 2.1) [83]. That trend is the opposite expected from the lower basic pK_a of a pyrazine ring compared to a pyridine ring [84], and may instead reflect stabilisation of the low-spin state of $[Fe(L^{37})_2]^{2+}$ by increased π-back-donation to the more electron-deficient pyrazine rings.

The salts $[Fe(L^{38})_2]X_2$ ($X^- = BF_4^-$ and ClO_4^-) both crystallise in the unusual tetragonal space group $I\bar{4}$ [85]. Again, this is not isostructural with the corresponding salts of $[Fe(L^1)_2]^{2+}$ (Section 3.2). Their spin transitions both show an unusual discontinuity at 50% conversion, which is most pronounced in the perchlorate salt (Fig. 9) [80]. Variable temperature crystallographic studies showed that, rather than reflecting a crystallographic phase change, this discontinuity is caused by an order:disorder transition of one of the two anion sites in the asymmetric unit. The small change in lattice pressure that results is enough to reduce the cooperativity of the transition for the remaining 50% of the iron centres [85]. This very unusual behaviour was successfully modelled by a new Ising-type theoretical model, that incorporates terms describing anion disorder [86]. The remaining two ligands in Scheme 8, L^{39} and L^{40}, both afford low-spin iron(II) complexes [80].

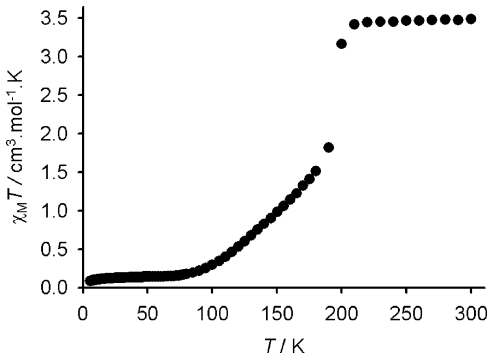

Fig. 9. Variable temperature magnetic susceptibility data for $[Fe(L^{38})_2][ClO_4]_2$ [80,85].

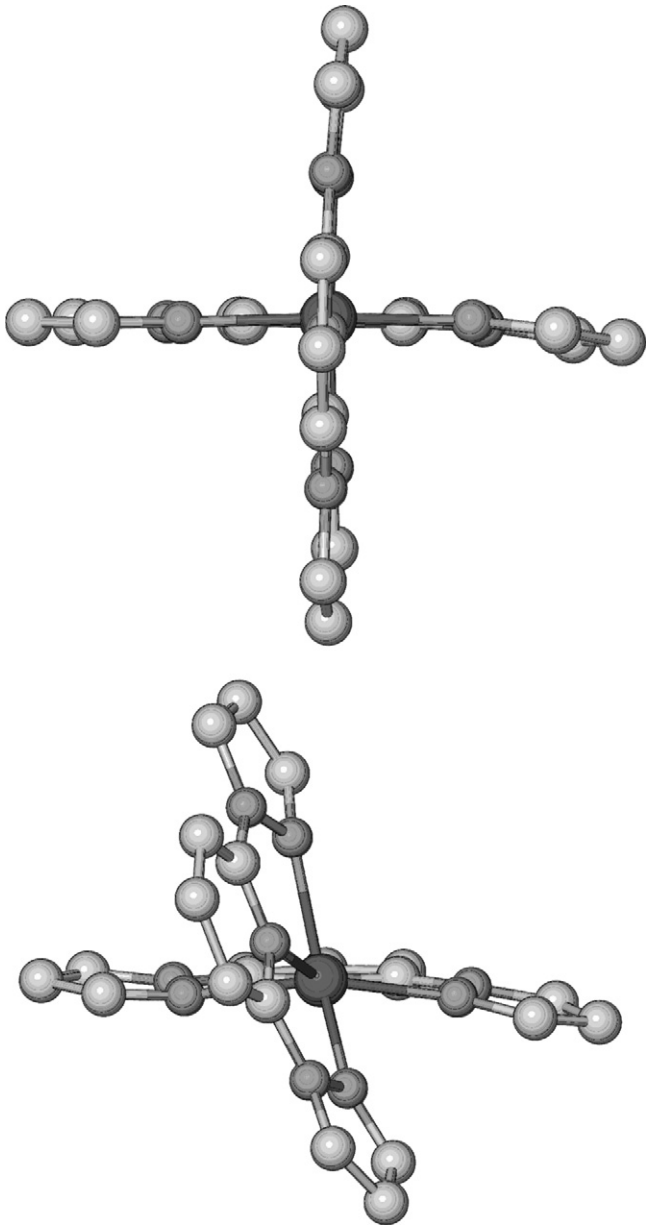

Fig. 10. Crystal structures of high-spin $[Fe(1\text{-bpp})_2][BF_4]_2$ (top) and $[Fe(1\text{-bpp})_2][PF_6]_2$ (bottom), illustrating the angular Jahn–Teller distortion adopted by the PF_6^- salt. The view in both cases is directly down one Fe–N{pyridine} bond.

5. Influence of coordination geometry on the occurrence of spin-crossover

One striking feature of the chemistry of $[Fe(1\text{-bpp})_2]^{2+}$ and its derivatives is the common observation of an unusual Jahn–Teller distortion in crystal structures of their high-spin complexes (Fig. 10). Rather than taking the more usual form of a structural elongation along one of the N{pyrazole}–Fe–N{pyrazole} vectors (as is shown by $[Cu(1\text{-bpp})_2]^{2+}$ [46,87]), the Jahn–Teller effect in the iron complexes often manifests itself as an angular structural distortion. This distortion has two components (Scheme 9): a twist of the plane of one ligand about its Fe–N{pyridine} bond, so that the dihedral angle between the least squares planes of the two ligands is <90° (θ in Scheme 9); and, a rotation of one ligand with respect to the other about the iron atom, so that the *trans*-N{pyridine}–Fe–N{pyridine} angle is <180° (ϕ in Scheme 9). The range of values observed for these parameters is shown in Table 3.

Table 3
Geometric parameters for high-spin salts of $[Fe(1\text{-bpp})_2]^{2+}$ and selected derivatives. Only structures that are unambiguously in a pure high-spin state at the temperature of measurement are included. See the text, and Scheme 9, for the definition of the parameters.

	α (°)	θ (°)	ϕ (°)	Σ (°)	Θ (°)	Reference
Spin-crossover on cooling						
$[Fe(1\text{-bpp})_2][BF_4]_2$	73.42 (6)	89.94 (2)	172.98 (7)	150.8 (2)	467	[31]
$[Fe(L^1)_2][BF_4]_2$	73.69 (9)	76.44	175.85 (9)	153.1 (3)	462	[59]
$[Fe(L^1)_2][BF_4]_2{\cdot}xH_2O$	73.8 (1)	76.37	175.3 (1)	154.8 (4)	460	[59]
$[Fe(L^3)_2][ClO_4]_2$	72.7 (1)	90	180	158.8 (4)	480	[35]
$[Fe(L^{15})_2][BF_4]_2$	73.23 (5)	90	180	153.2 (3)	470	[65]
$[Fe(L^{16})_2][BF_4]_2$	73.46 (4)	90	180	150.9 (2)	467	[65]
$[Fe(L^{20})_2][BF_4]_2$	73.8 (1)	89.71 (4)	178.4 (1)	147.6 (6)	454	[77]
$[Fe(L^{20})_2][ClO_4]_2$	73.8 (2)	89.36	177.4 (3)	147.7 (9)	458	[35]
β-$[Fe(L^{28})_2][BF_4]_2$	73.83 (7)	88.45	172.34 (8)	147.3 (3)	459	[71]
$[Fe(L^{37})_2][BF_4]_2{\cdot}3CH_3NO_2$	73.3 (1)	86.42 (4)	173.2 (1)	153.6 (4)	476	[80]
$[Fe(L^{38})_2][BF_4]_2$	73.52 (3)	90	180	150.3 (2)	460	[85]
$[Fe(L^{38})_2][ClO_4]_2$	72.97 (3)	90	180	156.1 (2)	480	[85]
High-spin at all temperatures – undistorted structure						
$[Fe(L^1)_2][SbF_6]_2$	73.7 (1)	87.66 (4)	178.0 (1)	148.8 (4)	460	[39]
$[Fe(L^5)_2][PF_6]_2{\cdot}CH_3CN{\cdot}0.5(C_2H_5)_2$[a]	73.6 (2)	84.19 (5)	175.0 (1)	149.4 (2)	465	[40]
	73.5 (2)	86.06 (6)	175.5 (2)	151.8 (2)	470	
	73.4 (2)	84.80 (6)	176.0 (2)	152.5 (2)	471	
	73.7 (2)	86.40 (5)	176.5 (2)	148.9 (2)	463	
$[Fe(L^{10})_2][BF_4]_2$	73.35 (7)	89.39 (2)	174.62 (7)	152.3 (2)	479	[40]
$[Fe(L^{22})_2][BF_4]_2{\cdot}2(C_2H_5)_2O$	74.07 (8)	88.27	175.4 (2)	144.7 (4)	453	[70]
High-spin at all temperatures – distorted structure						
$[Fe(1\text{-bpp})_2][PF_6]_2$	71.88 (4)	62.64 (1)	154.18 (7)	197.2 (2)	559	[30]
$[Fe(1\text{-bpp})_2][ClO_4]_2$	72.17 (4)	66.24 (2)	155.7 (1)	186.6 (2)	547	[40]
$[Fe(1\text{-bpp})_2][SbF_6]_2$	71.85 (5)	61.94 (2)	154.4 (1)	199.0 (3)	560	[40]
$[Fe(1\text{-bpp})_2][I_3]_2$[b]	72.7 (4)	87.3 (1)	159.6 (4)	167 (1)	513	[41]
	72.6 (4)	84.9 (1)	159.9 (4)	167 (1)	511	
	72.9 (4)	85.6 (1)	163.3 (4)	159 (1)	494	
	72.9 (4)	86.8 (1)	165.1 (4)	157 (1)	488	
	72.5 (4)	86.4 (1)	156.4 (4)	172 (1)	514	
	73.1 (4)	88.7 (1)	171.1 (5)	155 (1)	479	
$[Fe(1\text{-bpp})_2]I_{0.5}[I_3]_{1.5}$	72.7 (15)	89.92 (5)	156.0 (2)	172.8 (6)	522	[39]
$[Fe(1\text{-bpp})_2][Co(C_2B_9H_{11})_2]_2{\cdot}CH_3NO_2$[c]	73.3 (3)	87.03 (9)	159.6 (3)	157 (1)	482	[39]
α-$[Fe(L^7)_2][BF_4]_2$	73.2 (2)	61.15 (4)	176.3 (2)	177.0 (7)	479	[40]
β-$[Fe(L^7)_2][BF_4]_2$	73.13 (3)	62.30 (2)	180	176.8 (2)	482	[40]
$[Fe(L^9)_2][BF_4]_2{\cdot}3CH_3CN$[d]	72.89 (7)	66.28	180	168.7	481	[47]
	73.0 (1)	69.37	180	169.4	479	
$[Fe(L^{18})_2][BF_4]_2$	73.1 (1)	72.08 (3)	164.7 (1)	166.3 (3)	486	[40]
α-$[Fe(L^{18})_2][ClO_4]_2$	73.40 (8)	85.48 (2)	164.86 (8)	152.1 (3)	474	[64]
β-$[Fe(L^{18})_2][ClO_4]_2$	72.76 (7)	71.56 (2)	163.62 (7)	172.3 (2)	488	[64]
$[Fe(L^{22})_2][I_3]_2$	73.0 (4)	85.69	163.4 (3)	157 (1)	491	[78]
$[Fe(L^{22})_2][BPh_4]_2{\cdot}3CH_3NO_2{\cdot}(C_2H_5)_2O$	72.4 (2)	86.55	156.6 (1)	167.7 (5)	528	[78]
$[Fe(L^{22})_2][Ni(mnt)_2]_2$	73.4 (1)	74.38	166.1 (2)	169.7 (7)	479	[78]
α-$[Fe(L^{28})_2][BF_4]_2$	73.24 (7)	78.84	158.10 (7)	169.1 (2)	486	[71]
$[Fe(L^{37})_2][SbF_6]_2$	71.85 (7)	59.84 (3)	154.5 (1)	201.8 (4)	562	[82]
$[Fe(L^{37})_2][SbF_6]_2{\cdot}2CH_3NO_2$	72.9 (1)	84.66 (4)	163.2 (1)	161.0 (5)	485	[82]

[a] Four crystallographically independent molecules.
[b] Six crystallographically independent molecules.
[c] Molecule B at 150 K.
[d] Two crystallographically independent (half)-molecules.

Both components, together or in isolation, reduce the symmetry of the complex from D_{2d} to C_2. A DF calculation confirmed the Jahn–Teller effect as the cause of the unusual structure, and suggested that it is promoted by tridentate ligands with a narrow bite angle, like 1-bpp (whose bite angle 'α' is 72–74° in high-spin complexes, Table 3) [30]. Examples are known of distorted and undistorted molecules co-crystallising in the same lattice (Fig. 2) [39], and the same compound crystallising in distorted and undistorted high-spin polymorphs [64,71]. The most pronounced distortion discovered so far is in unsolvated $[Fe(L^{37})_2][SbF_6]_2$, which exhibits $\theta = 59.84(3)°$ and $\phi = 154.52(14)°$ [82].

Table 3 lists the θ and ϕ values for all crystallographically characterised high-spin compounds of the $[Fe(1\text{-bpp})_2]^{2+}$ type, grouped according to whether or not they undergo spin-crossover on cooling. A "distorted" high-spin compound is defined in the table, as one whose metric parameters lie outside the range found for spin-crossover high-spin centres. For comparison, the corresponding parameters for low-spin examples are also shown in Table 4, and the data in both tables are plotted in Fig. 11(top). The average ligand bite angle α is also included in the tables, as this has been used as a sensitive indicator of spin-state in these compounds [33,35,59,71,77]. High-spin compounds in this series Exhibit $72 < \alpha < 74°$, with the Jahn–Teller-distorted compounds giving values at the low end of that range, while the low-spin complexes show $79 < \alpha < 81°$. Crystal structures of compounds that are in a mixture of spin states will yield α values between those extremes.

Table 4
Geometric parameters for low-spin salts of $[Fe(1\text{-bpp})_2]^{2+}$ and its derivatives. Only examples that are unambiguously in a pure low-spin state at the temperature of measurement are included.

	α (°)	θ (°)	ϕ (°)	Σ (°)	Θ (°)	Reference
$[Fe(1\text{-bpp})_2][BF_4]_2$	80.08 (7)	89.40 (2)	178.15 (8)	86.1 (2)	282	[31]
$[Fe(1\text{-bpp})_2][BF_4]_2{\cdot}3CH_3NO_2$[a]	80.2 (1)	86.34 (4)	178.3 (1)	89.1 (4)	279	[30]
	80.0 (1)	89.14 (4)	177.5 (1)	86.5 (4)	283	
$[Fe(1\text{-bpp})_2][Co(C_2B_9H_{11})_2]_2{\cdot}CH_3NO_2$[b]	80.0 (3)	87.4 (1)	178.3 (3)	87 (1)	283	[39]
$[Fe(L^1)_2][BF_4]_2$	80.1 (2)	81.89	179.2 (2)	92.9 (5)	285	[59]
$[Fe(L^2)_2][BF_4]_2$	80.43 (7)	84.18 (2)	176.96 (7)	85.2 (2)	272	[29]
$[Fe(L^3)_2][BF_4]_2$	80.3 (1)	89.90 (3)	178.0 (1)	84.3 (4)	276	[35]
$[Fe(L^3)_2][ClO_4]_2$	79.8 (4)	89.86	175.8 (4)	89 (1)	288	[35]
$[Fe(L^8)_2][PF_6]_2{\cdot}2CH_3NO_2$	80.32 (8)	89.50 (2)	178.98 (8)	84.0 (3)	277	[28]
$[Fe(L^8)_2][FeCl_4]_2$[a]	80.7 (3)	89.85	178.7 (3)	81 (1)	269	[58]
	80.4 (3)	87.78	178.9 (3)	83 (1)	274	
$[Fe(L^{11})_2][BF_4]_2{\cdot}2CF_3C_2OH$	80.4 (1)	85.52 (3)	176.4 (1)	83.3 (3)	272	[49]
$[Fe(L^{13})_2][BF_4]_2{\cdot}1+xCH_3NO_2{\cdot}1-x(C_2H_5)_2O$[c]	80.4 (2)	81.32 (5)	178.7 (2)	89.5 (6)	270	[51]
	80.1 (2)	89.66 (4)	177.1 (2)	86.1 (6)	279	
	80.8 (2)	88.84 (4)	174.5 (2)	80.1 (7)	263	
$[Fe(L^{15})_2][BF_4]_2$	80.2 (2)	89.82 (4)	176.9 (3)	85.4 (8)	280	[65]
$[Fe(L^{17})_2][BF_4]_2{\cdot}2(CH_3)_2CO$	80.0 (2)	89.02 (4)	175.5 (2)	86.8 (5)	284	[52]
$[Fe(L^{20})_2][BF_4]_2$	79.54 (5)	89.87 (4)	177.3 (2)	91.2 (4)	297	[77]
$[Fe(L^{20})_2][ClO_4]_2$	79.2 (4)	89.98	177.7 (4)	94 (1)	306	[35]
$[Fe(L^{23})_2][BF_4]_2{\cdot}(CH_3)_2CO$	80.0 (3)	89.77	178.2 (3)	87 (1)	284	[69]
β-$[Fe(L^{28})_2][BF_4]_2$	79.97 (6)	88.65	178.22 (6)	87.3 (2)	286	[71]
$[Fe(L^{29})_2][ClO_4]_2$	80.10 (9)	88.20	178.6 (1)	86.1 (4)	281	[75]
$[Fe(L^{32})_2][ClO_4]_2$	80.0 (2)	87.98	177.7 (2)	87.2 (6)	285	[73]
$[Fe(L^{34})_2][ClO_4]_2$	79.78 (8)	87.67	178.3 (1)	89.0 (3)	291	[75]
$[FeH(L^{36})_2]_m[ClO_4]_{3m}{\cdot}mCH_3OH$	80.1 (2)	87.15	174.9 (2)	88.0 (7)	283	[72]
$[Fe(L^{37})_2][BF_4]_2{\cdot}3CH_3NO_2$	79.7 (1)	86.24 (3)	177.4 (1)	91.5 (4)	296	[80]
$[Fe(L^{37})_2][SbF_6]_2{\cdot}3CH_3NO_2$	80.2 (2)	88.59 (4)	178.6 (2)	85.5 (5)	281	[82]
$[Fe(L^{38})_2][BF_4]_2$	79.25 (4)	90	180	94.0 (2)	309	[85]
$[Fe\ (L^{38})_2][ClO_4]_2$	79.03 (3)	90	180	96.1 (2)	316	[85]
$[Fe(L^{39})_2][BF_4]_2$[a]	80.2 (1)	89.87 (3)	176.1 (1)	86.8 (4)	285	[80]
	80.3 (1)	88.09 (3)	179.5 (1)	84.5 (4)	279	
$[Fe(L^{40})_2][BF_4]_2{\cdot}5CH_3NO_2$	80.05 (7)	82.09 (4)	179.8 (2)	95.9 (3)	288	[80]

[a] Two crystallographically independent molecules.
[b] Molecule A at 150 K.
[c] Three crystallographically independent molecules. The θ values were calculated omitting the annelated indole C atoms.

It is clear that the θ and ϕ elements of the Jahn–Teller distortion can occur independently of each other (Fig. 11), and can vary significantly between different high-spin salts of the same compound (Table 3). As expected, the molecular structures of the low-spin examples show much less variation than the high-spin compounds [11]. Importantly, the high-spin compounds that exhibit spin-crossover on cooling have all θ and ϕ parameters lying close to the range as shown by the low-spin materials (Fig. 11). Comparison of the high- and low-spin structures of the same material shows that, in nearly all cases, spin-crossover is accompanied by a small increase in ϕ but essentially no change in θ (Table 5). That emphasises that a change in molecular size during a spin transition is accommodated by a solid lattice more readily than a change in molecular shape (θ has a greater influence than ϕ on the surface shape of the complex cation). The one exception to these observations is $[Fe(L^1)_2][BF_4]_2$, whose unusually large θ distortion for a high-spin spin-crossover complex is reflected in a significant change in this parameter in its (difficult to access) low-spin form (Table 5). It is tempting to speculate that this large structural rearrangement contributes to the unusually low temperature and slow kinetics shown by this spin transition [59]. All the high-spin com-

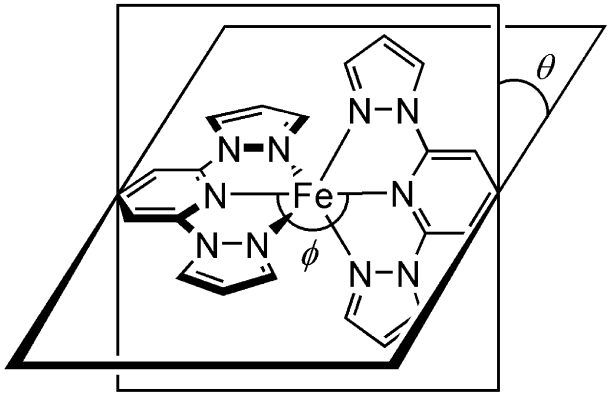

Scheme 9. The two components in the angular Jahn–Teller distortion in high-spin $[Fe(1\text{-bpp})_2]^{2+}$ complexes ($\theta \leq 90°$, $\phi \leq 180°$) [30].

Table 5
Structural changes taking place during spin-crossover for $[Fe(1\text{-bpp})_2]^{2+}$ and its derivatives, whose high-spin and low-spin crystal structures are available (Tables 3 and 4).

	$\lvert\Delta\theta\rvert$ (°)	$\lvert\Delta\phi\rvert$ (°)	$\Delta\Sigma$ (°)	$\Delta\Theta$ (°)	Reference
$[Fe(1\text{-bpp})_2][BF_4]_2$	0.5	5.2	64.7	185	[31]
$[Fe(L^1)_2][BF_4]_2$	5.5	3.4	60.2	177	[59]
$[Fe(L^3)_2][ClO_4]_2$	0.14	4.2	70	192	[35]
$[Fe(L^{15})_2][BF_4]_2$	0.18	3.1	67.8	190	[65]
$[Fe(L^{20})_2][BF_4]_2$	0.16	1.13	56.4	157	[77]
$[Fe(L^{20})_2][ClO_4]_2$	0.62	0.3	54	152	[35]
β-$[Fe(L^{28})_2][BF_4]_2$	0.2	5.9	60.0	173	[71]
$[Fe(L^{37})_2][BF_4]_2{\cdot}3CH_3NO_2$	0.18	4.2	62.1	180	[80]
$[Fe(L^{38})_2][BF_4]_2$	0	0	56.3	151	[85]
$[Fe(L^{38})_2][ClO_4]_2$	0	0	60.0	164	[85]

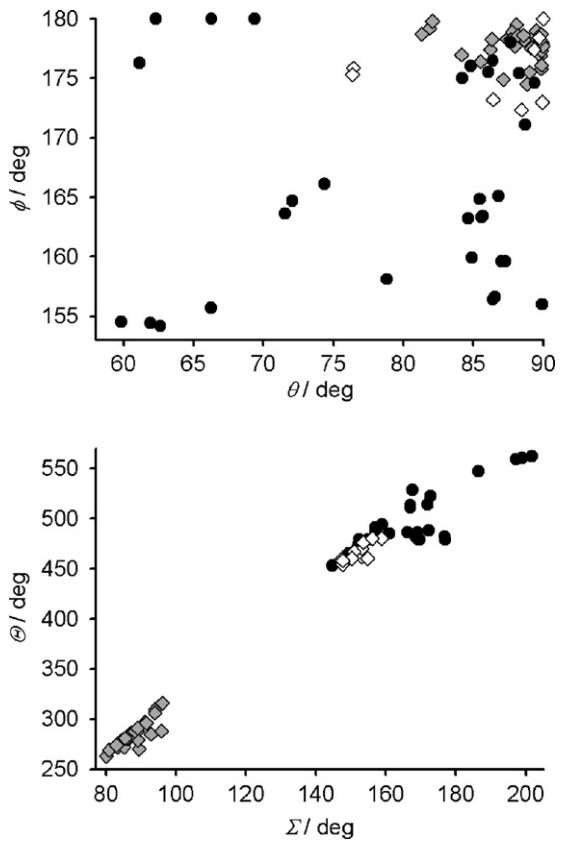

Fig. 11. Top: plot of the values of θ *vs.* ϕ for high-spin complexes that remain high-spin (●), spin-crossover complexes in their high-spin state (◊), and low-spin complexes (◆) from the $[Fe(1\text{-bpp})_2]^{2+}$ series (Scheme 9). Bottom: plot of the relationship between Σ and Θ for the same compounds. The data are taken from Tables 3 and 4.

pounds with $\theta < 76^\circ$ and/or $\phi < 172^\circ$, which is about two-thirds of the total, remain high-spin at all temperatures in the solid state. Presumably, the structural rearrangement required to bring their θ and ϕ parameters into the range required for a low-spin structure is too large to be accommodated by a rigid solid lattice.

The θ and ϕ parameters measure the disposition of the 1-bpp ligands around the iron centre. Since the *tris*-heterocyclic framework has some conformational flexibility, θ in particular is not always a good reflection of the structure of the N_6 donor sphere about the metal ion. The deviation of a metal centre from an ideal octahedral coordination geometry has been quantified using two different distortion indices. First is Σ, which measures local angular distortions of the octahedral donor set, Eq. (2):

$$\Sigma = \sum_{i=1}^{12} \left|90 - \alpha_i\right| \tag{2}$$

where α_i are the 12 *cis*-N–Fe–N angles at the metal centre [88]. Second is Θ, which defines more specifically the degree of trigonal distortion of the coordination geometry from an octahedron towards a trigonal prism, Eq. (3):

$$\Theta = \sum_{j=1}^{24} \left|60 - \beta_j\right| \tag{3}$$

where β_j are the 24 unique torsion angles between adjacent N donors on opposite triangular faces of the octahedron, measured along their common (pseudo)-three-fold axis [89,90]. An ideal octahedron would give Σ and $\Theta = 0$. These parameters for the compounds in this work are also listed in Tables 3 and 4, and plotted in Fig. 11 (bottom graph). As usual Σ and Θ are lower for the low-spin compounds in the Tables than for the high-spin ones, showing that the low-spin complexes have more regular coordination geometries. However, the values of Σ and Θ in the tables are up to four times higher than those from spin transition compounds with other ligand types [88–92]. This can again be attributed to the particularly narrow bite angle of the 1-bpp ligand.

There is a strong correlation between Σ and Θ in Tables 3 and 4, except for high-spin compounds showing moderate Jahn–Teller distortions (Fig. 11, bottom). These all give $\Theta \approx 480^\circ$, comparable to several of the undistorted high-spin compounds, while showing a range of values $157 \leq \Sigma \leq 177^\circ$ (Fig. 11). Table 3 shows that a decrease in either θ or ϕ results in an increase in Σ, but that Θ is much more sensitive to ϕ than to θ. Thus, reducing θ from 90° to 62° while maintaining ϕ around 180° in the two polymorphs of $[Fe(L^7)][BF_4]_2$ has essentially no effect on Θ, which adopts a value (480°) similar to those from undistorted high-spin complexes. Conversely, $[Fe(1\text{-bpp})_2]I_{0.5}[I_3]_{1.5}$ exhibits $\theta \approx 90^\circ$ but a strongly distorted $\phi = 156^\circ$, which leads to an increased $\Theta = 522^\circ$ (Table 3). Both these compounds give similar values of $\Sigma \approx 175^\circ$, around 20° higher than the undistorted high-spin complexes. Hence, Σ is a good measure of the overall magnitude of Jahn–Teller distortion in a $[Fe(1\text{-bpp})_2]^{2+}$ derivative, while Θ is a better indicator of whether it is the rotation and/or twisting distortion that is present in that compound.

If a crystal structure is not available, the existence of the angular Jahn–Teller distortion in a high-spin $[Fe(1\text{-bpp})_2]^{2+}$ derivative can often be inferred from variable temperature magnetic measurements. The magnitude of the zero-field splitting parameter $|D|$, which can be modelled from susceptibility data [93], is $12 \pm 1\,cm^{-1}$ in undistorted high-spin complexes but can be as low as $3\,cm^{-1}$ in distorted compounds [30,39,40,82]. A decrease in ϕ has a much stronger effect on $|D|$ than the value of θ, which probably reflects a reduction in magnetic anisotropy when the unique N{pyridine}–Fe–N{pyridine} molecular axis is lost [40]. Importantly, although this trend has been confirmed theoretically [30], magnetic susceptibility data are a convenient but inaccurate method for measuring $|D|$ [93]. So the true zero-field splittings of these compounds may be different from those given here. Mössbauer spectroscopy at routine temperatures is not so helpful to this problem. While the distorted complexes do appear to show higher values of δ and ΔE_Q than undistorted ones, the differences are partly masked by the normal temperature dependence of the Mössbauer parameters in high-spin iron(II) compounds [40]. Mössbauer measurements at liquid helium temperatures would be required to delineate the spectroscopic signature of the angular distortion in more detail.

Although most examples of this unusual Jahn–Teller structure are $[Fe(1\text{-bpp})_2]^{2+}$ derivatives, it is not unique to this system. High-spin $[Fe(terpy)_2]^{2+}$ derivatives are rare but exhibit a similar angularly distorted structure in the crystal [15,58,94], while it is also occasionally seen in $[Fe(3\text{-bpp})_2]^{2+}$ (Scheme 1) [95] and complexes of other tridentate *tris*-imine ligands with first row transition ions [96].

6. Influence of structure on the cooperativity of spin-crossover

The influence of structure on the cooperativity of spin-crossover is slowly being elucidated [88], although it has been difficult to generalise conclusions about one set of materials to other classes of compound. The scale of the problem is illustrated by the alcohol solvates $[Fe(pic)_3]Cl_2 \cdot ROH$ (R = one of six different alkyl groups) [97]. Although they are not perfectly isostructural, these compounds all adopt the same basic crystal packing arrangement, based around a particular 2D hydrogen bonding topology. Despite that similarity,

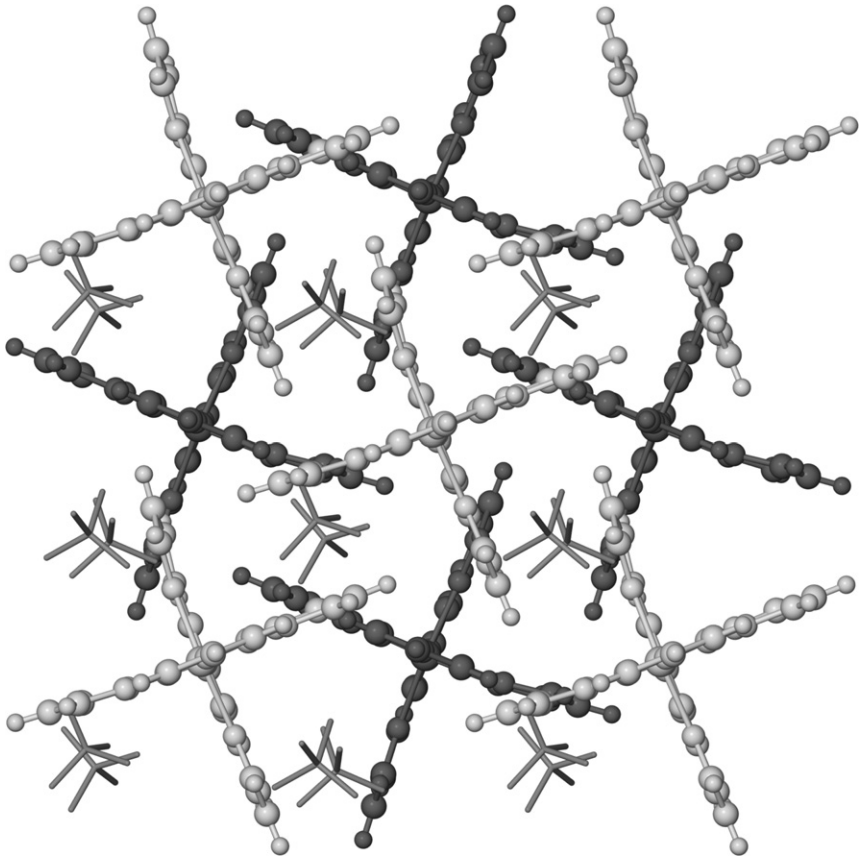

Fig. 12. Partial packing diagram of $[Fe(1\text{-bpp})_2][BF_4]_2$, showing the terpyridine embrace structure motif. Molecules in the two unique cation layers, which alternate down the unit cell *c* axis, are coloured pale and dark. Only one orientation of the disordered BF_4^- anions is shown, which are de-emphasised for clarity.

their spin-transition regimes are very different, ranging from a conventional gradual spin-crossover (R = Me); a more abrupt transition with a discontinuity at 50% conversion (R = Et); an unsymmetrically structured transition with a partial hysteresis loop (R = *i*Pr); and, two materials that remain high-spin at all temperatures (R = *n*Pr and *t*Bu). While the structural origin of the individual features of the transitions in these materials are now mostly understood [60,98], a unified explanation of why they behave differently has not yet appeared.

We noted that six compounds from the $[Fe(1\text{-bpp})_2]^{2+}$ series exhibit abrupt spin transitions with small hysteresis loops, that are essentially identical in form [65]. Two of these, $[Fe(1\text{-bpp})_2][BF_4]_2$ [27,30] and α-$[Fe(L^{15})_2][BF_4]_2$ [52,65], are shown in Figs. 1 and 5. The other examples are $[Fe(L^3)_2][ClO_4]_2$ [35], $[Fe(L^{16})_2][BF_4]_2$ [52,65] and the BF_4^- and ClO_4^- salts of $[Fe(L^{37})_2]^{2+}$ [80,81]. The degree of structural resemblance of these six compounds is comparable to that in the $[Fe(pic)_2]Cl_2{\cdot}ROH$ system. They all form versions of the "terpyridine embrace" crystal lattice [99], described below, but differ in their more detailed structural chemistry (Table 6). Of the compounds in the Table, only α-$[Fe(L^{15})_2][BF_4]_2$ and $[Fe(L^{16})_2][BF_4]_2$ are isostructural to each other in both their high-spin and low-spin forms [52,65]. Also, five of the six compounds undergo crystallographic phase changes during spin-crossover ($[Fe(1\text{-bpp})_2][BF_4]_2$ is the exception), but at least three different types of phase change are involved including two different changes in space group [35,52], and a unit cell expansion in the same space group [81]. The cooperativity of spin-crossover in these compounds is clearly unaffected by the presence or absence of a crystallographic phase change.

The terpyridine embrace structure is common in crystalline $[M(terpy)_2]^{2+}$ salts and related compounds, and contains 2D layers of D_{2d} symmetric cations linked through four-fold interlacing of the their distal heterocyclic rings (pyrazolyl rings in $[Fe(1\text{-bpp})_2]^{2+}$, Fig. 12) [99]. Since each molecule in a layer is aligned the same way the individual layers are polar, although both centrosymmetric and polar versions of the structure are known (depending on whether molecules in different layers are related by an inversion centre, or a different symmetry element). Cations within the layers interact strongly with each other through face-to-face and edge-to-face interactions between heterocyclic groups. The anions occupy cavities between the layers, which are in van der Waals contact only. The different versions of this structure vary according to the internal symmetry within the layers and the symmetry relating adjacent layers, which are usually stacked along the crystallographic *c* direction [99].

It is reasonable to suggest that the consistent cooperativity in the compounds in Table 6, is primarily transmitted in two dimensions through the terpyridine embrace layers. There are several pieces of circumstantial evidence supporting that hypothesis. First, is that

Table 6
Transition temperatures and crystallographic symmetry for the compounds in this work exhibiting similar abrupt spin-crossover [65].

	$T_{½}\downarrow$ (K)	$T_{½}\uparrow$ (K)	High-spin space group	Low-spin space group
$[Fe(1\text{-bpp})_2][BF_4]_2$	258	261	$P2_1$ ($Z=2$)	$P2_1$ ($Z=2$)
$[Fe(L^3)_2][ClO_4]_2$	231	234	$P\bar{4}2_1c$	$P2_12_12_1$
α-$[Fe(L^{15})_2][BF_4]_2$	200	203	$P\bar{4}2_1c$	$P2_1$ ($Z=2$)
$[Fe(L^{16})_2][BF_4]_2$	252	254	$P\bar{4}2_1c$	$P2_1$ ($Z=2$)[a]
$[Fe(L^{37})_2][BF_4]_2$	218	221	$P2_1$ ($Z=4$)[a]	$P2_1$ ($Z=6?$)[a]
$[Fe(L^{37})_2][ClO_4]_2$	203	206	$P2_1$ ($Z=2$)	$P2_1$ ($Z=4$)

[a] Tentative – from preliminary powder diffraction data only.

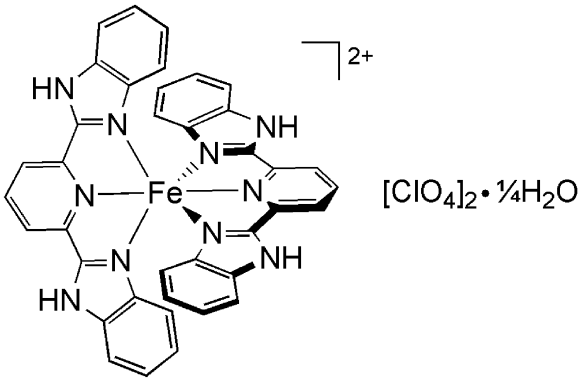

Scheme 10. [Fe(bzimpy)][ClO_4]$_2$·1/4H_2O [101].

changes in anion disorder are unlikely to be relevant to the cooperativity because, where available, crystal structures just above and below the transition temperature show the same degree of anion disorder [27,52]. Second, is that doping the larger perchlorate anion into [Fe(1-bpp)$_2$][BF_4]$_2$ has a greater influence on the interlayer spacing than on the dimensions within the layers themselves, and has no measurable effect on the cooperativity of the transition [31]. Lastly, is the difference between α- and β-[Fe(L^{15})$_2$][BF_4]$_2$ (Fig. 5). The crystal packing in the β polymorph closely resembles the terpyridine embrace structure with two unique cation sites 'A' and 'B', only one of which (site B) is spin-crossover active below room temperature [52]. The nearest neighbours of site B within the layers are all of the inactive A type, so the B cations are well isolated from each other within the layers. Conversely, the nearest neighbours of site B between the layers are also of the B type. The very gradual spin-crossover exhibited by β-[Fe(L^{15})$_2$][BF_4]$_2$ (Fig. 5) strongly implies that cooperativity between the layers is weak, and hence intralayer interactions play a major role in the cooperativity of the terpyridine embrace compounds in Table 6 [52].

There are some data from other iron(II) complexes that also support these suggestions. Although terpyridine embrace crystals are less common in [Fe(3-bpp)$_2$]$^{2+}$ salts (Scheme 1), one spin-crossover salt of that complex does adopt this structure type in its high-spin state. That is [Fe(3-bpp)$_2$][NCSe]$_2$, whose spin transition strongly resembles those in Table 6, occurring abruptly at 232 K with a 2 K hysteresis loop [100]. The compound [Fe(bzimpy)$_2$][ClO_4]$_2$·1/4H_2O (bzimpy = 2,6-di(benzimidazol-2-yl)pyridine, Scheme 10) is also relevant, in showing an abrupt spin transition at 403 K with a 12 K hysteresis loop. The low-spin form of this material also crystallises in four-fold cation layers, that closely resemble the terpyridine embrace motif [101]. It is possible that the larger hysteresis in its spin-crossover, compared to the materials in Table 6, may reflect the more extensive π–π stacking within its four-fold layers mediated by the annelated benzimidazole arms.

Two pairs of compounds provide exceptions to the above discussion, however. First is [Fe(L^{38})$_2$]X_2 (X^- = BF_4^- and ClO_4^-) [80], which crystallise in one of the more unusual versions of the terpyridine embrace [85]. Their spin transitions are clearly distinct from the compounds in Table 6, occurring in two steps (Fig. 9) with the discontinuity being controlled by changes in anion disorder (Section 4.3) [85,86]. Importantly, the steric bulk of the L^{38} methyl groups pushes neighbouring molecules in the cation layers apart so no π–π interactions can form. Hence, the face-to-face intermolecular distance between nearest neighbour pyrazole groups in the layers in these crystals is 5.7 Å [85], rather than the more usual 3.4–3.6 Å found in the compounds in Table 6. Therefore it is reasonable that intralayer cooperativity between cations in these compounds should be reduced, and anion-mediated interactions become dominant.

The behaviour of the second pair of compounds, [Fe(L^{20})$_2$]X_2 (X^- = BF_4^- and ClO_4^-), is more ambiguous. These also crystallise in the terpyridine embrace, now with normal (3.4–3.6 Å) face-to-face spacings between pyrazole rings within the layers, but exhibit less cooperative transitions (Fig. 7) [35]. The cations and anions in these compounds are linked by strong O–H···Y (Y = O or F) hydrogen bonds, and spin-crossover is accompanied by a crystallographic ordering of the anions and ligand hydroxymethyl groups [77]. It may be that this coupling of structural changes in the cation and anion sites perturbs the intermolecular cooperativity in these materials. Alternatively, it is noteworthy that the structural change at the metal ion during spin-crossover in [Fe(L^{20})$_2$]X_2, as measured by the distortion indices $\Delta\phi$, $\Delta\Sigma$ and $\Delta\Theta$, is significantly smaller than for the three compounds in Table 6 for which these data are available (Table 5) [35,77]. The smaller change in molecular structure during spin-crossover for the L^{20} complex salts could easily result in weaker cooperativity [89,90]. The possible relevance of $\Delta\Sigma$ and $\Delta\Theta$ in this system is also apparent in [Fe(L^{38})$_2$]X_2 from the previous paragraph [80,85]. The BF_4^- salt of this complex exhibits both a less cooperative spin transition, and smaller $\Delta\Sigma$ and $\Delta\Theta$ values (Table 5), than its isostructural perchlorate analogue.

A good correlation between $\Delta\Theta$ and spin-crossover cooperativity has also been noted in another class of iron(II) compound [90]. Discussion of cooperativity in other [Fe(1-bpp)$_2$]$^{2+}$ derivatives like those in Table 1 is more difficult, however, since few of them have been crystallographically characterised in both their high-spin and low-spin states (Table 5). Notably, [Fe(L^{20})$_2$]X_2 (X^- = BF_4^- and ClO_4^-) [35,77] and β-[Fe(L^{28})$_2$][BF_4]$_2$ [71] give similar transition widths of 60–80 K despite having somewhat different $\Delta\Sigma$ and $\Delta\Theta$ values (Table 6), but this is too small a sample of compounds to make that a meaningful observation.

The facile angular Jahn–Teller distortion discussed in Section 5 may also have a bearing on spin-crossover in some of these materials. For example, the coordination polymers [Fe(μ-L^{27})]$_n$$X_{2n}$·$n$$H_2O$ (X^- = BF_4^- and ClO_4^-) and [Fe(μ-L^{33})]$_n$[BF_4]$_{2n}$ contain chains of [Fe(1-bpp)$_2$]$^{2+}$ centres linked by 1,2-ethylenediyl and 1,4-phenylenediyl groups, respectively. All these materials are poorly crystalline, but their magnetic susceptibility properties are very different (Fig. 13). Solid [Fe(μ-L^{33})]$_n$[BF_4]$_{2n}$ is mostly low-spin at room temperature and exhibits a typical, essentially complete spin transition on warming, centred at 323 K [74]. In contrast, the L^{27}-containing polymers are high-spin at room temperature and undergo extremely gradual spin-crossover to only 25–35% completeness on cooling from 300 to 100 K [68]. Although the more flexible saturated linker in L^{27} may also be relevant, we propose that the poor functionality of [Fe(μ-L^{27})]$_n$$X_{2n}$·$n$$H_2O$ might relate to its high-spin nature under the conditions of precipitation. This could

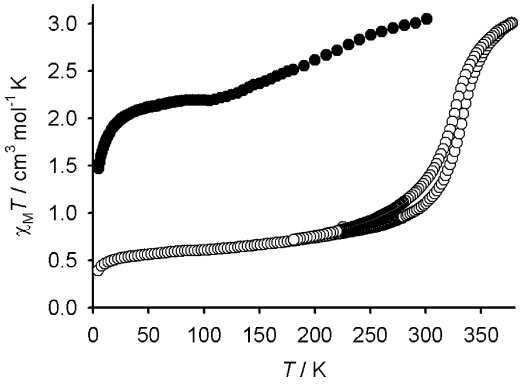

Fig. 13. Variable temperature magnetic susceptibility data for [Fe(μ-L^{27})]$_n$[ClO_4]$_{2n}$·$n$$H_2O$ (●) [68] and [Fe(μ-L^{33})]$_n$[BF_4]$_{2n}$ (○) [74]. Data for the L^{33} compound were measured in both cooling and warming mode.

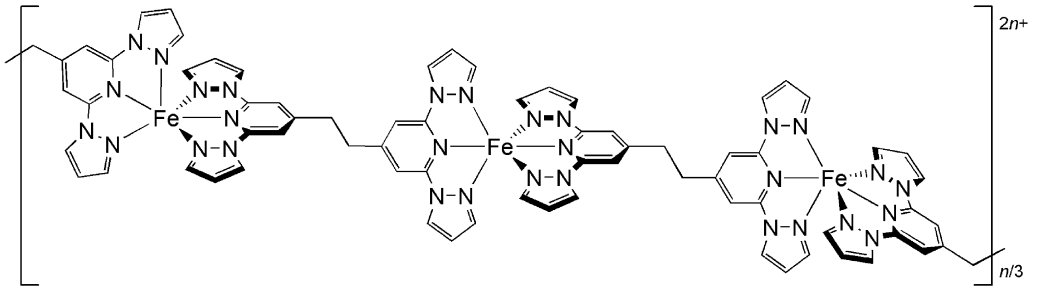

Scheme 11. Proposed structure of $[Fe(\mu\text{-}L^{27})]_nX_{2n}{\cdot}nH_2O$ ($X^- = BF_4^-$ and ClO_4^-), with a random distribution of undistorted and Jahn–Teller distorted iron centres (Fig. 10) [68].

lead to a random, frozen-in distribution of distorted and undistorted high-spin iron centres (Scheme 11), which would account for the poor completeness of the transitions. The productive, undistorted sites would experience inhomogeneous local environments in the amorphous solid, as well as being separated from each other along the polymer chains by the unproductive distorted iron centres. Both those aspects would lead to the very poor cooperativity observed. Since $[Fe(\mu\text{-}L^{33})]_n[BF_4]_{2n}$ is low-spin under the conditions of precipitation it will contain exclusively undistorted low-spin iron centres, explaining the complete and cooperative spin transition observed on heating (Fig. 13) [72]. Some other poorly soluble, non-crystalline complexes from the $[Fe(1\text{-}bpp)_2]^{2+}$ series that are high-spin at room temperature (for example, salts of $[Fe(L^{12})_2]^{2+}$ [50], $[Fe(L^{25})_2]^{2+}$ and $[Fe(L^{26})_2]^{2+}$ [68]) also show very poor spin-crossover behaviour, for possibly the reasons described here.

A similar explanation has also been invoked to explain the irreversible high-temperature spin transitions undergone by some coordination polymers of $[Fe(terpy)_2]^{2+}$ centres in liquid-crystalline media [15]. Since crystalline high-spin $[Fe(terpy)_2]^{2+}$ derivatives are also Jahn–Teller-distorted [58,94], the transitions were proposed to convert undistorted low-spin iron centres into distorted high-spin sites, which are then trapped in their high-spin states upon recooling. Such a structural rearrangement is only possible in a fluid medium, however, and cannot take place in solid polymers like $[Fe(\mu\text{-}L^{33})]_n[BF_4]_{2n}$.

7. Solid solutions of functional complexes in a terpyridine embrace lattice

The robustness of the terpyridine embrace structure, even in the presence of competing supramolecular interactions, has already been remarked upon [102]. We have made use of that property to prepare solid solutions between $[Fe(1\text{-}bpp)_2][BF_4]_2$ and the fluorophore $[Ru(terpy)_2][BF_4]_2$ [32]. Isomorphous metal dilution studies (cocrystallisation of two complexes containing the same ligands and/or anions but different metal ions) have played an important role in the development of models for the propagation of cooperative spin transitions [24]. However, this is the first example of the co-crystallisation of a spin-crossover compound with a completely different complex molecule. This represents an alternative approach to the use of double salts of functional cations and anions, for the preparation of multifunctional spin-crossover materials (Section 1) [22,23,78,95].

While these two compounds crystallise in different space groups ($P2_1$ and Cc, respectively), they are both different versions of the terpyridine embrace structure (Fig. 12) and their crystal packing is visually almost indistinguishable. The solid solutions $[Fe(1\text{-}bpp)_2]_n[Ru(terpy)_2]_{1-n}[BF_4]_2$ show some small phase separation when $n \approx 0.5$, but other compositions are phase-pure, adopting the $P2_1$ lattice when $n \geq 0.47$ and the Cc lattice when $n \leq 0.28$. There is no evidence for segregation of $[Fe(1\text{-}bpp)_2]^{2+}$ centres into the $P2_1$ lattice, and of $[Ru(terpy)_2]^{2+}$ into the Cc lattice, in compositions containing both crystal phases. Importantly there is no intermolecular exchange of 1-bpp and terpy ligands between the iron and ruthenium centres in the crystallisation solvent used by ^1H NMR. So, the solid solutions will contain purely $[Fe(1\text{-}bpp)_2]^{2+}$ and $[Ru(terpy)_2]^{2+}$, with no significant mixed-ligand contaminants [32].

The spin transitions in $[Fe(1\text{-}bpp)_2]_n[Ru(terpy)_2]_{1-n}[BF_4]_2$ are typical for doped spin-crossover materials [24], becoming more gradual as n decreases and the iron centres become more dilute (Fig. 14) [32]. The mid-point temperature of the spin transition $T_{½}$ shows an unusual trend, however in that $T_{½}$ decreases only slightly with n when $n > 0.57$, before showing a small increase upon further dilution (Fig. 14) [24]. We attribute this discontinuity to the different space groups adopted by the solid solutions: predominantly $P2_1$ when $n \geq 0.47$, and Cc when $n = 0.28$. Presumably the Cc structure stabilises the low-spin state of $[Fe(1\text{-}bpp)_2]^{2+}$ to a slightly greater degree than the $P2_1$ lattice. Comparable behaviour is shown by $[Fe_mZn_{1-m}(ptz)_6][BF_4]_2$ (ptz = 1-propyltetrazole), where a crystallographic phase change accompanying spin-crossover in the pure iron compound is suppressed when $m < 0.44$. This change in the structural chemistry of the spin transition leads to a discontinuous decrease in $T_{½}$ at that composition [103].

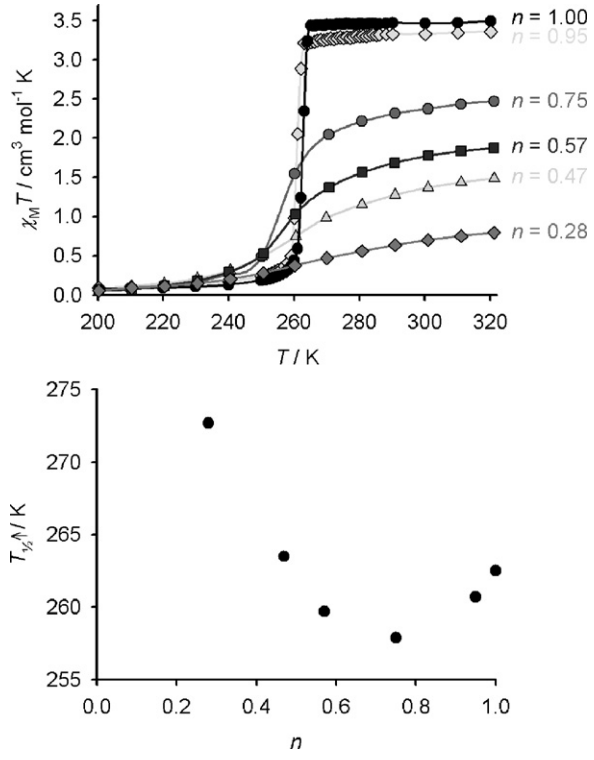

Fig. 14. Top: Warming mode magnetic data for $[Fe(1\text{-}bpp)_2]_n[Ru(terpy)_2]_{1-n}[BF_4]_2$. Data for each compound are linked by a spline curve for clarity. Bottom: Compositional dependence of $T_{½}$ for $[Fe(1\text{-}bpp)_2]_n[Ru(terpy)_2]_{1-n}[BF_4]_2$ [32].

Preliminary solid-state fluorescence measurements showed that the solid solutions gave a typical $[Ru(terpy)_2]^{2+}$ emission spectrum below 100 K when $n \leq 0.47$, albeit with a strongly reduced fluorescence intensity compared to the neat ruthenium complex, but are not emissive near room temperature [32]. While fluorescence and spin-crossover are not observed under the same temperature regime in these materials, the fact that we can co-crystallise two such molecules in a homogeneous phase while retaining their functionalities is still extremely promising. Since $[Ru(terpy)_2]^{2+}$ is a different shape from $[Fe(1\text{-}bpp)_2]^{2+}$ and is 10% larger by volume, the tolerance of the terpyridine embrace for two such different cations is remarkable for a molecular lattice.

A set of isomorphous solid solutions $[Fe_mNi_{1-m}(1\text{-}bpp)_2][BF_4]_2$ was also studied, for purposes of comparison with the mixed-cation materials. The iron/nickel samples behaved completely typically for metal-diluted spin-crossover solids, and again implied that cations in the terpyridine embrace lattice are quite insensitive to small changes in their local environment [32] (*c.f.* the mixed-anion materials $[Fe(1\text{-}bpp)_2][BF_4]_x[ClO_4]_{2-x}$, Section 6 [31]).

8. The LIESST effect

Spin-crossover and low-spin materials from the $[Fe(1\text{-}bpp)_2]^{2+}$ family regularly exhibit the LIESST effect (Section 1) upon irradiation with green laser light at 10 K or below (Fig. 15) [31,34,35,52,59,69]. Photoconversions of 80–100% during irradiation are common for samples that exhibit thermal spin-crossover below room temperature [31,34,35,52,59], while even materials that are low-spin at room temperature can give up to 40% conversion [52,69]. Only one pair of compounds in this article has been reported to fail in the LIESST experiment, namely $[Fe(L^{38})_2]X_2$ ($X^- = BF_4^-$ and ClO_4^-) which relaxed instantaneously back to their low-spin ground state when the laser was turned off [85]. The reason for this unique behaviour, for a $[Fe(1\text{-}bpp)_2]^{2+}$ complex, is uncertain although it may be relevant that those compounds are fluorescent [63]. The thermal relaxation temperatures of the metastable high-spin states generated by irradiation (T_{LIESST}, Fig. 15) are usually between 65 and 100 K [34,35,52,59]. That is at the high end of the typical range of values for molecular compounds [4].

The availability of a series of chemically similar compounds with different thermal spin-crossover temperatures has been useful for the development of the theory of LIESST phenomena. Létard et al. have proposed that the thermal stability of the LIESST excited state in a solid material is a function of molecular structure, rather than the wider crystal lattice [4]. For chemically similar compounds the

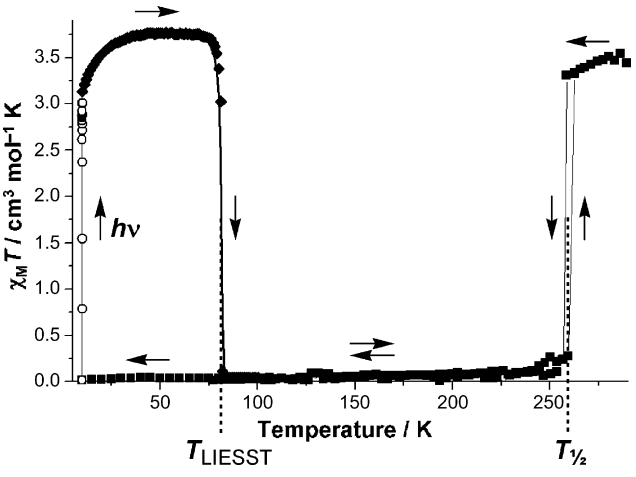

Fig. 15. The LIESST behaviour of $[Fe(1\text{-}bpp)_2][BF_4]_2$ [34,35]. The sample was cooled, irradiated at 10 K until its magnetisation saturated, then rewarmed.

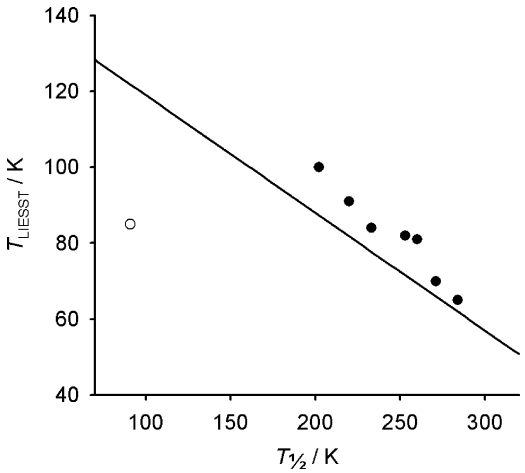

Fig. 16. Relationship between $T_{½}$ and T_{LIESST} for nine compounds in the $[Fe(1\text{-}bpp)_2]^{2+}$ series (there are two data points overlaid at $T_{½} = 201$, $T_{LIESST} = 100$ K) [34,35,52]. The solid line shows the previously proposed linear correlation between $T_{½}$ and T(LIESST) for other complexes of meridional tridentate ligands [4,106]. The outlying data point (○) is for $[Fe(L^1)_2][BF_4]_2 \cdot xH_2O$ [59].

T_{LIESST} values follow the empirical relationship Eq. (4).

$$T_{LIESST} = T_0 - 0.3T_{½} \quad (4)$$

The form of Eq. (4) reflects Hauser's previously proposed inverse energy gap law, where a reduction in $T_{½}$ reflects a stabilisation of the high-spin state relative to the low-spin state. That leads to a reduced driving force for relaxation of the same high-spin state, when it is kinetically trapped in the LIESST experiment, and a corresponding increase in T_{LIESST} [104]. Experimentally, T_0 is a function of the rigidity of the ligand donor sphere bound to the iron centre. Thus, complexes of monodentate ligands follow Eq. (4) with $T_0 = 100$ K [105], complexes of bidentate ligands show $T_0 = 120$ K [105], and tridentate *tris*-heterocyclic ligands give $T_0 = 150$ K [106]. Eight complexes from the $[Fe(1\text{-}bpp)_2]^{2+}$ series have now been found to obey Eq. (4), with the same value of $T_0 = 150$ K that had been previously proposed using a different set of materials (Fig. 16) [34,35,52].

The importance of the 1-bpp ligand framework in controlling T_{LIESST} is emphasised by the following comparison. T_{LIESST} for $[Fe(1\text{-}bpp)_2][BF_4]_2$ ($T_{½} = 260$ K) is 81 K (Fig. 15), in general agreement with the value predicted by Eq. (4) with the appropriate T_0 value of 150 K [34,35]. Conversely $[Fe(L^{41})_2][ClO_4]_2 \cdot H_2O$ (L^{41} = 2,6-di[pyrazol-1-ylmethyl]pyridine, Scheme 12) exhibits a very similar $T_{½}$, = 250 K, but a much lower T_{LIESST} of 38 K [107]. That reflects the increased conformational flexibility of the L^{41} ligands, whose heterocyclic donor groups are separated by methylene spacers rather than being directly linked. In effect, the LIESST response from $[[Fe(L^{41})_2][ClO_4]_2 \cdot H_2O$ resembles that expected from a complex of

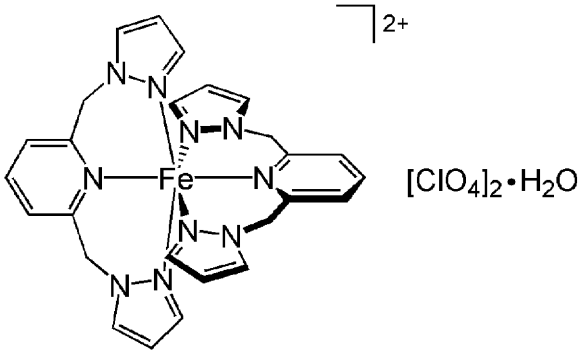

Scheme 12. $[Fe(L^{41})][ClO_4]_2 \cdot H_2O$ [107].

six independent monodentate heterocyclic donors, rather than that of two rigid tridentate ligand domains as in the 1-bpp compound.

Although the thermal stability of a LIESST excited state in a solid molecular compound is only slightly perturbed by its extended lattice, the lattice has a strong influence on the rate of the LIESST relaxation reaction. Kinetic data have been measured for LIESST relaxation in eight $[Fe(1\text{-bpp})_2][BF_4]_2$ complex salts, all of which adopt the terpyridine embrace structure. These compounds all show strongly self-accelerating LIESST relaxation kinetics, implying that relaxation of one molecule makes the relaxation of its neighbours more favourable. That can be modelled by a sigmoidal equation, to account for intermolecular cooperativity [4]. The activation energies for relaxation derived from these data are all $E_a = 10^4\,cm^{-1}$, while cooperativity energies span the range $40 \leq E_a^* \leq 390\,cm^{-1}$ [35,52]. These are at the high ends of the values that are usually observed in molecular materials [108,109]. The resultant implication, that intermolecular cooperativity in the terpyridine embrace lattice is strong, is supported by two additional observations. First, the two terpyridine embrace materials with the least abrupt thermal spin transitions, $[Fe(L^{20})_2]X_2$ ($X^- = BF_4^-$ and ClO_4^-), also yield the lowest values of relaxation cooperativity E_a^* [35]. Second is that the two compounds in this work that have been measured in this way and do not crystallise in the terpyridine embrace lattice, $[Fe(L^1)_2][BF_4]_2{\cdot}xH_2O$ [59] and $[Fe(L^{17})_2][BF_4]_2$ [52], exhibit much less cooperative relaxation kinetics.

LIESST experiments have also been performed on single crystals of some of the compounds in this work. Three of the terpyridine embrace crystals, $[Fe(1\text{-bpp})_2][BF_4]_2$ [33] and both salts of $[Fe(L^{20})_2]X_2$ ($X^- = BF_4^-$ and ClO_4^-) [35,77], undergo complete low → high-spin conversion without significant decomposition when irradiated on the diffractometer at 30 K. The thermal relaxation temperatures of these excited crystals, as determined from unit cell measurements at increasing temperatures, perfectly matched those shown by bulk powders of the compounds. Full structure determinations were achieved on all three excited crystals, allowing two different electronic states of the same molecules to be structurally characterised at the same temperature. The molecular structures of the LIESST high-spin states at 30 K, and the corresponding thermally populated high-spin states at room temperature, were identical within experimental error for all three compounds. That contrasts with other experiments of this type, where small but real differences in metric parameters between the two structures are often observed [110]. That has been attributed to the effects of anisotropic contraction of the crystal on cooling, leading to the molecules experiencing different lattice pressures at the very different temperatures of the two experiments, although it might also reflect incomplete photoconversion in the crystal during irradiation [111]. In any case, it is reasonable that the effectively axial symmetry of the terpyridine embrace structure ($a \simeq b$, $\beta \simeq 90°$), with the molecular and crystalline unique axes almost perfectly coincident, should lead to a relatively small variation in the distribution of lattice pressure in these three compounds at different temperatures. Crystallographic characterisation of the LIESST high-spin states of $[Fe(L^1)_2][BF_4]_2{\cdot}xH_2O$ ($x = 0$ and 1/3, see below) were also achieved [59].

The LIESST effect in $[Fe(L^1)_2][BF_4]_2{\cdot}xH_2O$ is particularly unusual [59]. As described in Section 3.2 this solid undergoes a kinetically slow spin transition, at a temperature depending on its water content x. The transition proceeds through a mixed spin-state intermediate crystal phase, that the material becomes trapped in if it is cooled too quickly. Laser irradiation of the low-spin or the mixed-spin phase at 10 K affords 100% conversion to the same high-spin state, that decays to the fully low-spin form at $T_{LIESST} = 81$ K (Fig. 17). There are two novel aspects to this behaviour. Usually, a LIESST excited state relaxes back to the same phase from which it was generated [106,108,112]. However, the high-spin excited state generated from the mixed-spin phase of $[Fe(L^1)_2][BF_4]_2{\cdot}xH_2O$ decays instead to the fully low-spin state, apparently violating the principle of microscopic reversibility (Fig. 17). Kinetic measurements confirmed that there is no hidden intermediate in the relaxation process, which proceeds cleanly from high-spin to low-spin without passing through the mixed-spin intermediate [59]. In addition, the LIESST relaxation in $[Fe(L^1)_2][BF_4]_2{\cdot}xH_2O$ takes place in one step, where Eq. (4) implies there should be two (reflecting the two steps in the thermal transition) (Fig. 17) [35,113]. Hence, although the thermal spin transition is sensitive to the water content of the material, the LIESST relaxation reaction is not.

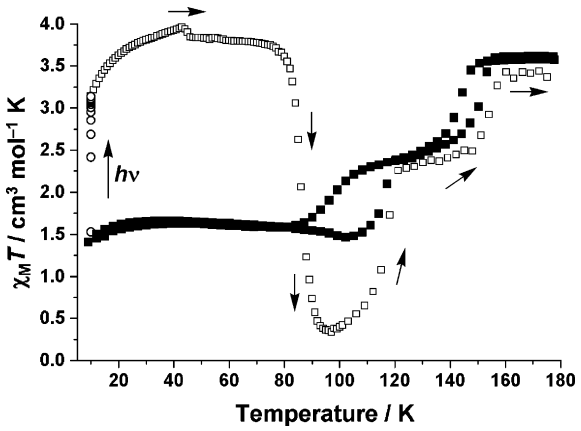

Fig. 17. The LIESST behaviour of $[Fe(L^1)_2][BF_4]_2{\cdot}xH_2O$ [59]. The sample was irradiated at 10 K until its magnetisation saturated (○), then warmed (□). The compound's thermal spin transition is also shown, for comparison (■).

These observations all imply that high → low-spin crossover under thermal (thermodynamic control) and LIESST relaxation (kinetic control) conditions have become decoupled from each other in this material. Although the structural basis for this novel behaviour remains uncertain, it is noteworthy that this is the only material from the $[Fe(1\text{-bpp})_2]^{2+}$ series so far whose LIESST properties are not described by Eq. (4) (Fig. 16). It may be relevant that Eq. (4) predicts $T_{LIESST} \approx 118$ K for hydrated $[Fe(L^1)_2][BF_4]_2{\cdot}xH_2O$ ($x = 1/3$), which is above its $T_{1/2}$ value of 105 K. That physical impossibility is avoided by the different pathways of the thermal and LIESST spin transitions, which allows the material to access a lower T_{LIESST} value.

9. Conclusions

The range of substituents that can be added to the periphery of the $[Fe(1\text{-bpp})_2]^{2+}$ cation gives it two features that set it apart from other workhorses in spin-crossover research. First, is the availability of a series of spin-transition materials whose structural chemistry is similar enough to allow trends in their behaviour to be identified [65]. Second, is the ability to incorporate additional functionality at a remote site from the coordinated metal ion which, for example, has allowed the synthesis of linear polymers of $[Fe(1\text{-bpp})_2]^{2+}$ centres [68,74]. There is strong potential for the synthesis of more multifunctional molecules based on this ligand scaffold [70,73]. These advantages are partly offset, however, by the prevalence of the angular Jahn–Teller distortion in this system which traps many solid $[Fe(1\text{-bpp})_2]^{2+}$ derivatives in their high-spin state (Section 5).

The consistent form of the spin transitions in $[Fe(1\text{-bpp})_2]^{2+}$ and $[Fe(3\text{-bpp})_2]^{2+}$ salts that adopt the terpyridine embrace lattice (Fig. 12), represents the one of the first occasions that a particular spin-crossover functionality can be attributed to a particular form of crystal packing [65]. Although definitive proof is still to be obtained, there is strong circumstantial evidence that cooperativity in these compounds is transmitted between molecules in two

dimensions, within the four-fold layers of the lattice [31,65]. The only other spin-crossover materials that have been studied in this amount of detail are compounds of type $[Fe(NCS)_2L_2]$ (L = a bidentate bis-imine donor ligand), whose cooperativity, $T_{½}$ and T_{LIESST} all correlate well with $\Delta\Theta$ (Eq. (3), Section 5) [88,90]. There is some indication that $\Delta\Theta$ may also have a bearing on the cooperativity in $[Fe(1\text{-bpp})_2]^{2+}$ compounds, although more examples that have been structurally characterised in both spin states are required to confirm that suggestion (Table 5). The LIESST behaviour of $[Fe(1\text{-bpp})_2]^{2+}$ derivatives is also notably consistent [35,52], with the important exception of $[Fe(L^1)_2][BF_4]_2{\cdot}xH_2O$ [59] (Fig. 16). The complicated phase behaviour and anomalous LIESST relaxation of that compound make it one of the most complex spin-crossover materials yet to have been discovered.

Remarkably the terpyridine embrace structure type is robust enough that it can accommodate two completely different complex cations, $[Fe(1\text{-bpp})_2]^{2+}$ and $[Ru(terpy)_2]^{2+}$, in a homogeneous phase [32]. Since metal terpyridine complexes can exhibit various types of functionality [114], including spin-crossover [8], this is potentially a powerful new method for preparing multifunctional switchable materials.

Supplementary data

Full crystallographic data for $[Fe(1\text{-bpp})_2][I_3]_2$ [41], which has not been published elsewhere, are available on request from the Cambridge Crystallographic Data Centre, 12 Union Road, Cambridge CB2 1EZ, UK (http://www.ccdc.cam.ac.uk/). The CCDC deposition number is 734793.

Acknowledgements

The author's work discussed in this article was carried out by Drs. Joanne Holland, Jérôme Elhaïk, Christopher Pask, Ruth Pritchard and Clare Tovee, and Ms. Rufeida Mohammed. Help from Dr. Victoria Money and Professor Judith Howard FRS (University of Durham), Drs. Chiara Carbonera and Jean-François Létard (ICMCB, Bordeaux), and other collaborators cited in the references is gratefully acknowledged. Dr. Mario Ruben (Institut für Nanotechnologie, Forschungszentrum Karlsruhe) is thanked for providing the magnetic data from $[Fe(\mu\text{-}L^{33})]_n[BF_4]_{2n}$ in Fig. 13. The author is grateful to the Research Centre for Materials Science, Nagoya University, for a sabbatical that allowed the writing of this article.

Crystal structure figures in this article were produced with the program *XSEED* [115] (which incorporates *POVRAY* [116]), using coordinates down-loaded from the Cambridge Crystallographic Database [117] where necessary. Graphs were prepared using *SIGMAPLOT* [118].

References

[1] P. Gütlich, H.A. Goodwin, Spin Crossover in Transition Metal Compounds I–III, Top. Curr. Chem., vol. 233–235, 2004.
[2] (a) P. Gütlich, A. Hauser, H. Spiering, Angew. Chem. Int. Ed. 33 (1994) 2024;
(b) P. Gütlich, Y. Garcia, H.A. Goodwin, Chem. Soc. Rev. 29 (2000) 419;
(c) P. Gütlich, P.J. van Koningsbruggen, F. Renz, Struct. Bond. (Berlin) 107 (2004) 27;
(d) J.A. Real, A.B. Gaspar, M.C. Muñoz, Dalton Trans. (2005) 2062;
(e) O. Sato, J. Tao, Y.-Z. Zhang, Angew. Chem. Int. Ed. 46 (2007) 2152.
[3] M.A. Halcrow, Chem. Soc. Rev. 37 (2008) 278.
[4] (a) J.-F. Létard, P. Guionneau, O. Nguyen, J.S. Costa, S. Marcén, G. Chastanet, M. Marchivie, L. Goux-Capes, Chem. Eur. J. 11 (2005) 4582;
(b) J.-F. Létard, J. Mater. Chem. 16 (2006) 2550.
[5] P. Gütlich, V. Ksenofontov, A.B. Gaspar, Coord. Chem. Rev. 249 (2005) 1811.
[6] (a) M.A. Halcrow, Polyhedron 26 (2007) 3523;
(b) A. Bousseksou, G. Molnár, J.A. Real, K. Tanaka, Coord. Chem. Rev. 251 (2007) 1822;
(c) K.S. Murray, Eur. J. Inorg. Chem. (2008) 3101;
(d) B. Weber, E.-G. Jäger, Eur. J. Inorg. Chem. (2009) 465;
(e) I. Šalitroš, N.T. Madhu, R. Boča, J. Pavlik, M. Ruben, Monatsh. Chem. 140 (2009) 695.
[7] (a) M. Nakamura, Coord. Chem. Rev. 250 (2006) 2271;
(b) M. Nihei, T. Shiga, Y. Maeda, H. Oshio, Coord. Chem. Rev. 251 (2007) 2606.
[8] I. Krivokapic, M. Zerara, M.L. Daku, A. Vargas, C. Enachescu, C. Ambrus, P. Tregenna-Piggott, N. Amstutz, E. Krausz, A. Hauser, Coord. Chem. Rev. 251 (2007) 364.
[9] For selected recent examples see:
(a) V. Ksenofontov, A.B. Gaspar, G. Levchenko, B. Fitzsimmons, P. Gütlich, J. Phys. Chem. B 108 (2004) 7723;
(b) P. Angaridis, F.A. Cotton, C.A. Murillo, D. Villagrán, X. Wang, J. Am. Chem. Soc. 127 (2005) 5008;
(c) G.G. Morgan, K.D. Murnaghan, H. Müller-Bunz, V. McKee, C.J. Harding, Angew. Chem. Int. Ed. 45 (2006) 7192;
(d) A.E. Ashley, R.T. Cooper, G.G. Wildgoose, J.C. Green, D. O'Hare, J. Am. Chem. Soc. 130 (2008) 15662;
(e) M.D. Walter, C.D. Sofield, C.H. Booth, R.A. Andersen, Organometallics 28 (2009) 2005.
[10] O. Kahn, J. Kröber, C. Jay, Adv. Mater. 4 (1992) 718.
[11] E. König, Prog. Inorg. Chem. 35 (1987) 527.
[12] (a) A. Bousseksou, G. Molnár, P. Demont, J. Menegotto, J. Mater. Chem. 13 (2003) 2069;
(b) S. Bonhommeau, T. Guillon, L.M.L. Daku, P. Demont, J.S. Costa, J.-F. Létard, G. Molnár, A. Bousseksou, Angew. Chem. Int. Ed. 45 (2006) 1625.
[13] M. Matsuda, H. Tajima, Chem. Lett. 36 (2007) 700.
[14] (a) J.-F. Létard, O. Nguyen, H. Soyer, C. Mingotaud, P. Delhaes, O. Kahn, Inorg. Chem. 38 (1999) 3020;
(b) Y. Galyametdinov, V. Ksenofontov, A. Prosvirin, I. Ovchinnikov, G. Ivanova, P. Gütlich, W. Haase, Angew. Chem. Int. Ed. 40 (2001) 4269;
(c) M. Seredyuk, A.B. Gaspar, V. Ksenofontov, S. Reiman, Y. Galyametdinov, W. Haase, E. Rentschler, P. Gütlich, Chem. Mater. 18 (2006) 2513;
(d) S. Hayami, N. Motokawa, A. Shuto, N. Masuhara, T. Someya, Y. Ogawa, K. Inoue, Y. Maeda, Inorg. Chem. 46 (2007) 1789;
(e) S. Hayami, R. Moriyama, A. Shuto, Y. Maeda, K. Ohta, K. Inoue, Inorg. Chem. 46 (2007) 7692;
(f) S. Hayami, Na. Motokawa, A. Shuto, R. Moriyama, N. Masuhara, K. Inoue, Y. Maeda, Polyhedron 26 (2007) 2375;
(g) M. Seredyuk, A.B. Gaspar, V. Ksenofontov, Y. Galyametdinov, J. Kusz, P. Gütlich, J. Am. Chem. Soc. 130 (2008) 1431;
(h) M. Seredyuk, A.B. Gaspar, V. Ksenofontov, Y. Galyametdinov, J. Kusz, P. Gütlich, Adv. Funct. Mater. 18 (2008) 2089;
(i) A.B. Gaspar, V. Ksenofontov, Y. Galyametdinov, M. Verdaguer, F. Villain, P. Gütlich, Inorg. Chem. 47 (2008) 10232.
[15] (a) Y. Bodenthin, U. Pietsch, H. Mhwald, D.G. Kurth, J. Am. Chem. Soc. 127 (2005) 3110;
(b) Y. Bodenthin, G. Schwarz, Z. Tomkowicz, T. Geue, W. Haase, U. Pietsch, D.G. Kurth, J. Am. Chem. Soc. 131 (2009) 2934.
[16] (a) E. Coronado, J.R. Galán-Mascarós, M. Monrabal-Capilla, J. García-Martínez, P. Pardo-Ibáñez, Adv. Mater. 19 (2007) 1359;
(b) T. Forestier, S. Mornet, N. Daro, T. Nishihara, S. Mouri, K. Tanaka, O. Fouché, E. Freysz, J.-F. Létard, Chem. Commun. (2008) 4327;
(c) F. Volatron, L. Catala, E. Rivière, A. Gloter, O. Stéphan, T. Mallah, Inorg. Chem. 47 (2008) 6584;
(d) I. Boldog, A.B. Gaspar, V. Martínez, P. Pardo-Ibañez, V. Ksenofontov, A. Bhattacharjee, P. Gütlich, J.A. Real, Angew. Chem. Int. Ed. 47 (2008) 6433;
(e) J. Larionova, L. Salmon, Y. Guari, A. Tokarev, K. Molvinger, G. Molnár, A. Bousseksou, Angew. Chem. Int. Ed. 47 (2008) 8236;
(f) T. Forestier, A. Kaiba, S. Pechev, D. Denux, P. Guionneau, C. Etrillard, N. Daro, E. Freysz, J.-F. Létard, Chem. Eur. J. 15 (2009) 6122.
[17] (a) S. Cobo, G. Molnár, J.A. Real, A. Bousseksou, Angew. Chem. Int. Ed. 45 (2006) 5786;
(b) G. Molnár, S. Cobo, J.A. Real, F. Carcenac, E. Daran, C. Vieu, A. Bousseksou, Adv. Mater. 19 (2007) 2163;
(c) G. Agustí, S. Cobo, A.B. Gaspar, G. Molnár, N. Ould Moussa, P.Á. Szilágyi, V. Pálfi, C. Vieu, M.C. Muñoz, J.A. Real, A. Bousseksou, Chem. Mater. 20 (2008) 6721;
(d) M. Cavallini, I. Bergenti, S. Milita, G. Ruani, I. Salitros, Z.-R. Qu, R. Chandrasekar, M. Ruben, Angew. Chem. Int. Ed. 47 (2008) 8597.
[18] O. Kahn, C.J. Martinez, Science 279 (1998) 44.
[19] (a) M. Matsuda, H. Isozaki, H. Tajima, Chem. Lett. 37 (2008) 374;
(b) M. Matsuda, H. Isozaki, H. Tajima, Thin Solid Films 517 (2008) 1465.
[20] R.N. Muller, L. Vander Elst, S. Laurent, J. Am. Chem. Soc. 125 (2003) 8405.
[21] A.B. Gaspar, V. Ksenofontov, M. Seredyuk, P. Gütlich, Coord. Chem. Rev. 249 (2005) 2661.
[22] See e.g;
(a) S. Dorbes, L. Valade, J.A. Real, C. Faulmann, Chem. Commun. (2005) 69;
(b) C. Faulmann, S. Dorbes, B. Garreau de Bonneval, G. Molnár, A. Bousseksou, C.J. Gomez-Garcia, E. Coronado, L. Valade, Eur. J. Inorg. Chem. (2005) 3261;
(c) K. Takahashi, H.-B. Cui, Y. Okano, H. Kobayashi, Y. Einaga, O. Sato, Inorg. Chem. 45 (2006) 5739;
(d) C. Faulmann, K. Jacob, S. Dorbes, S. Lampert, I. Malfant, M.-L. Doublet, L. Valade, J.A. Real, Inorg. Chem. 46 (2007) 8548.
[23] K. Takahashi, H.-B. Cui, Y. Okano, H. Kobayashi, H. Mori, H. Tajima, Y. Einaga, O. Sato, J. Am. Chem. Soc. 130 (2008) 6688.
[24] A. Hauser, J. Jeftić, H. Romstedt, R. Hinek, H. Spiering, Coord. Chem. Rev. 190–192 (1999) 471.
[25] (a) S. Hayami, Z. Gu, Y. Einaga, Y. Kobayasi, Y. Ishikawa, Y. Yamada, A. Fujishima, O. Sato, Inorg. Chem. 40 (2001) 3240;

(b) J.S. Costa, P. Guionneau, J.-F. Létard, J. Phys. Conf. Ser. 21 (2005) 67.
[26] A. Hauser, C. Enachescu, M.L. Daku, A. Vargas, N. Amstutz, Coord. Chem. Rev. 250 (2006) 1642.
[27] J.M. Holland, J.A. McAllister, Z. Lu, C.A. Kilner, M. Thornton-Pett, M.A. Halcrow, Chem. Commun. (2001) 577.
[28] J.M. Holland, S.A. Barrett, C.A. Kilner, M.A. Halcrow, Inorg. Chem. Commun. 5 (2002) 328.
[29] M.A. Halcrow, Coord. Chem. Rev. 249 (2005) 2880.
[30] J.M. Holland, J.A. McAllister, C.A. Kilner, M. Thornton-Pett, A.J. Bridgeman, M.A. Halcrow, J. Chem. Soc. Dalton Trans. (2002) 548.
[31] C. Carbonera, C.A. Kilner, J.-F. Létard, M.A. Halcrow, Dalton Trans. (2007) 1284.
[32] C.A. Tovee, C.A. Kilner, J.A. Thomas, M.A. Halcrow, CrystEngComm, in press, doi:10.1039/b904528g.
[33] V.A. Money, I. Radosavljevic Evans, M.A. Halcrow, A.E. Goeta, J.A.K. Howard, Chem. Commun. (2003) 158.
[34] V.A. Money, J.S. Costa, S. Marcén, G. Chastanet, J. Elhaïk, M.A. Halcrow, J.A.K. Howard, J.-F. Létard, Chem. Phys. Lett. 391 (2004) 273.
[35] C. Carbonera, J.S. Costa, V.A. Money, J. Elhaïk, J.A.K. Howard, M.A. Halcrow, J.-F. Létard, Dalton Trans. (2006) 3058.
[36] M.B. Darkhovskii, A.L. Tchougréeff, J. Phys. Chem. A 108 (2004) 6351.
[37] N. Suaud, M.-L. Bonnet, C. Boilleau, P. Labèguerie, N. Guihéry, J. Am. Chem. Soc. 131 (2009) 715.
[38] M. Enamullah, W. Linert, Thermochim. Acta 388 (2002) 401.
[39] J. Elhaïk, C.A. Kilner, M.A. Halcrow, Dalton Trans. (2006) 823.
[40] J. Elhaïk, D.J. Evans, C.A. Kilner, M.A. Halcrow, Dalton Trans. (2005) 1693.
[41] $[Fe(1\text{-}bpp)_2][I_3]_2$ was isolated under the same conditions used for $[Fe(1\text{-}bpp)_2]I_{0.5}[I_3]_{1.5}$ [39], but using a different batch of FeI_2 starting material. Crystal data for $[Fe(1\text{-}bpp)_2][I_3]_2$: $C_{22}H_{18}FeI_6N_{10}$, M_r 1239.71, triclinic, $P\bar{1}$, a = 19.4467(12), b = 24.1237(14), c = 24.9584(15) Å, α = 80.400(4)°, β = 68.204(4)°, γ = 79.977(4)°, V = 10638.7(11) Å^3, Z = 12, $\mu(MoK_\alpha)$ = 5.677 mm^{-1}, T = 293(2)K, 141833 reflections collected, 43667 unique (R_{int} = 0.048), $R_1(F)$, $I > 2\sigma(I)$ = 0.066, $wR_2(F^2)$, all data = 0.223, S = 1.009.
[42] D.L. Jameson, K.A. Goldsby, J. Org. Chem. 55 (1990) 4992.
[43] J.M. Holland, C.A. Kilner, M. Thornton-Pett, M.A. Halcrow, Polyhedron 20 (2001) 2829.
[44] X. Sun, Z. Yu, S. Wu, W.-J. Xiao, Organometallics 24 (2005) 2959.
[45] M.A. Halcrow, Dalton Trans. (2009) 2059.
[46] N.K. Solanki, E.J.L. McInnes, F.E. Mabbs, S. Radojevic, M. McPartlin, N. Feeder, J.E. Davies, M.A. Halcrow, Angew. Chem. Int. Ed. 37 (1998) 2221.
[47] L. Han, M. Nihei, H. Oshio, Polyhedron 24 (2005) 2409.
[48] M.J. Remuiñán, H. Román, M.T. Alonso, J.C. Rodríguez-Ubis, J. Chem. Soc. Perkin Trans. 2 (1993) 1099.
[49] R. Pritchard, C.A. Kilner, S.A. Barrett, M.A. Halcrow, Inorg. Chim. Acta, in press, doi:10.1016/j.ica.2009.01.022.
[50] C.A. Tovee, J.A. Thomas, M.A. Halcrow, unpublished data.
[51] R. Pritchard, C.A. Kilner, M.A. Halcrow, Tetrahedron Lett. 50 (2009) 2484.
[52] R. Pritchard, H. Lazar, S.A. Barrett, C.A. Kilner, S. Asthana, C. Carbonera, J.-F. Létard, M.A. Halcrow, Dalton Trans., in press, doi:10.1039/b907094j.
[53] G. Zoppellaro, M. Baumgarten, Eur. J. Org. Chem. (2005) 2888 and 4201 (correction).
[54] R. Pritchard, Ph.D. thesis, University of Leeds, 2008.
[55] R. Mohammed, M.A. Halcrow, unpublished data.
[56] (a) J. Elguero, E. Gonzalez, R. Jacquier, Bull. Soc. Chim. Fr. (1968) 5009;
(b) J. Catalan, M. Menéndez, J. Elguero, Bull. Soc. Chim. Fr. (1985) 30.
[57] C.A. Kilner, M.A. Halcrow, Acta Crystallogr. Sect. C 62 (2006) m437.
[58] F. Pelascini, M. Wesolek, F. Peruch, A. De Cian, N. Kyritsakas, P.J. Lutz, J. Kress, Polyhedron 23 (2004) 3193.
[59] V.A. Money, C. Carbonera, J. Elhaïk, M.A. Halcrow, J.A.K. Howard, J.-F. Létard, Chem. Eur. J. 13 (2007) 5503.
[60] D. Chernyshov, M. Hostettler, K.W. Törnroos, H.-B. Bürgi, Angew. Chem. Int. Ed. 42 (2003) 3285.
[61] (a) T. Nakamoto, A. Bhattacharjee, M. Sorai, Bull. Chem. Soc. Jpn. 77 (2004) 921;
(b) J. Kusz, P. Gütlich, H. Spiering, Top. Curr. Chem. 234 (2004) 129 (and references therein).
[62] (a) G. Ritter, E. König, W. Irler, H.A. Goodwin, Inorg. Chem. 17 (1978) 224;
(b) R. Hinek, H. Spiering, P. Gütlich, A. Hauser, Chem. Eur. J. 2 (1996) 1435;
(c) N. Moliner, A.B. Gaspar, M.C. Muñoz, V. Niel, J. Cano, J.A. Real, Inorg. Chem. 40 (2001) 3986;
(d) A.B. Gaspar, M.C. Muñoz, N. Moliner, V. Ksenofontov, G. Levchenko, P. Gütlich, J.A. Real, Monatsh. Chem. 134 (2003) 285.
[63] J. Elhaïk, Ph.D. thesis, University of Leeds, 2004.
[64] J. Elhaïk, C.A. Kilner, M.A. Halcrow, CrystEngComm 7 (2005) 151.
[65] R. Pritchard, C.A. Kilner, M.A. Halcrow, Chem. Commun. (2007) 577.
[66] (a) J.C. Rodríguez-Ubis, R. Sedano, G. Barroso, O. Juanes, E. Brunet, Helv. Chim. Acta 80 (1997) 86 and 621 (correction);;
(b) E. Brunet, O. Juanes, R. Sedano, J.C. Rodríguez-Ubis, Photochem. Photobiol. Sci. 1 (2002) 613.
[67] (a) J. Yuan, G. Wang, K. Majima, K. Matsumoto, Anal. Chem. 73 (2001) 1869;
(b) J. Yuan, M. Tan, G. Wang, J. Luminesc. 106 (2004) 91.
[68] J. Elhaïk, C.M. Pask, C.A. Kilner, M.A. Halcrow, Tetrahedron 63 (2007) 291.
[69] M. Nihei, T. Maeshima, Y. Kose, H. Oshio, Polyhedron 26 (2007) 1993.
[70] M. Nihei, L. Han, H. Oshio, J. Am. Chem. Soc. 129 (2007) 5312.
[71] M. Haryono, F.W. Heinemann, K. Petukhov, K. Gieb, P. Müller, A. Grohmann, Eur. J. Inorg. Chem. (2009) 2136.
[72] C. Rajadurai, F. Schramm, S. Brink, O. Fuhr, M. Ghafari, R. Kruk, M. Ruben, Inorg. Chem. 45 (2006) 10019.
[73] R. Chandrasekar, F. Schramm, O. Fuhr, M. Ruben, Eur. J. Inorg. Chem. (2008) 2649.
[74] C. Rajadurai, O. Fuhr, R. Kruk, M. Ghafari, H. Hahn, M. Ruben, Chem. Commun. (2007) 2636.
[75] N.T. Madhu, I. Salitros, F. Schramm, S. Klyatskaya, O. Fuhr, M. Ruben, C. R. Chimie 11 (2008) 1166.
[76] C. Rajadurai, Z. Qu, O. Fuhr, B. Gopalan, R. Kruk, M. Ghafari, M. Ruben, Dalton Trans. (2007) 3531.
[77] V.A. Money, J. Elhaïk, M.A. Halcrow, J.A.K. Howard, Dalton Trans. (2004) 1516.
[78] M. Nihei, L. Han, H. Tahira, H. Oshio, Inorg. Chim. Acta 361 (2008) 3926.
[79] M. Loï, M.W. Hosseini, A. Jouaiti, A. De Cian, J. Fischer, Eur. J. Inorg. Chem. (1999) 1981.
[80] J. Elhaïk, V.A. Money, S.A. Barrett, C.A. Kilner, I.R. Evans, M.A. Halcrow, Dalton Trans. (2003) 2053.
[81] V.A. Money, I.R. Evans, J. Elhaïk, M.A. Halcrow, J.A.K. Howard, Acta Crystallogr. Sect. B 60 (2004) 41.
[82] C.A. Kilner, M.A. Halcrow, Polyhedron 25 (2006) 235.
[83] S.A. Barrett, M.A. Halcrow, unpublished data.
[84] A. Albert, R. Goldacre, J. Phillips, J. Chem. Soc. (1948) 2240.
[85] V.A. Money, J. Elhaïk, I.R. Evans, M.A. Halcrow, J.A.K. Howard, Dalton Trans. (2004) 65.
[86] D. Chernyshov, N. Klinduhov, K.W. Törnroos, M. Hostettler, B. Vangdal, H.-B. Bürgi, Phys. Rev. B 76 (2007) 014406.
[87] (a) M.A. Leech, N.K. Solanki, M.A. Halcrow, J.A.K. Howard, S. Dahaoui, Chem. Commun. (1999) 2245;
(b) N.K. Solanki, M.A. Leech, E.J.L. McInnes, F.E. Mabbs, J.A.K. Howard, C.A. Kilner, J.M. Rawson, M.A. Halcrow, J. Chem. Soc. Dalton Trans. (2002) 1295;
(c) G.S. Beddard, M.A. Halcrow, M.A. Hitchman, M.P. de Miranda, C.J. Simmons, H. Stratemeier, Dalton Trans. (2003) 1028.
[88] P. Guionneau, M. Marchivie, G. Bravic, J.-F. Létard, D. Chasseau, Top. Curr. Chem. 234 (2004) 97.
[89] J.K. McCusker, A.L. Rheingold, D.N. Hendrickson, Inorg. Chem. 35 (1996) 2100.
[90] M. Marchivie, P. Guionneau, J.-F. Létard, D. Chasseau, Acta Crystallogr. Sect. B 61 (2005) 25.
[91] H.Z. Lazar, T. Forestier, S.A. Barrett, C.A. Kilner, J.-F. Létard, M.A. Halcrow, Dalton Trans. (2007) 4276.
[92] R. Pritchard, S.A. Barrett, C.A. Kilner, M.A. Halcrow, Dalton Trans. (2008) 3159.
[93] R. Boča, Coord. Chem. Rev. 248 (2004) 757.
[94] E.C. Constable, G. Baum, E. Bill, R. Dyson, R. van Eldik, D. Fenske, S. Kaderli, D. Morris, A. Neubrand, M. Neuburger, D.R. Smith, K. Wieghardt, M. Zehnder, A.D. Zuberbühler, Chem. Eur. J. 5 (1999) 498.
[95] M. Clemente-León, E. Coronado, M.C. Giménez-López, F.M. Romero, Inorg. Chem. 46 (2007) 11266.
[96] (a) G. Stupka, L. Gremaud, G. Bernardinelli, A.F. Williams, Dalton Trans. (2004) 407;
(b) B.S. Hammes, B.J. Damiano, P.H. Tobash, M.J. Hidalgo, G.P.A. Yap, Inorg. Chem. Commun. 8 (2005) 513.
[97] M. Hostettler, K.W. Törnroos, D. Chernyshov, B. Vangdal, H.-B. Bürgi, Angew. Chem. Int. Ed. 43 (2004) 4589.
[98] (a) B.A. Katz, C.E. Strouse, J. Am. Chem. Soc. 101 (1979) 6214;
(b) K.W. Törnroos, M. Hostettler, D. Chernyshov, B. Vangdal, H.-B. Bürgi, Chem. Eur. J. 12 (2006) 6207.
[99] (a) M.L. Scudder, H.A. Goodwin, I.G. Dance, New J. Chem. 23 (1999) 695;
(b) J. McMurtrie, I. Dance, CrystEngComm 7 (2005) 216.
[100] (a) K.H. Sugiyarto, M.L. Scudder, D.C. Craig, H.A. Goodwin, Aust. J. Chem. 53 (2000) 755;
(b) C. Baldé, C. Desplanches, P. Gütlich, E. Freysz, J.-F. Létard, Inorg. Chim. Acta 361 (2008) 3529.
[101] (a) R. Boča, P. Baran, L. Dlháň, H. Fuess, W. Haase, F. Renz, W. Linert, I. Svoboda, R. Werner, Inorg. Chim. Acta 260 (1997) 129;
(b) R. Boča, M. Boča, L. Dlháň, K. Falk, H. Fuess, W. Haase, R. Jaroščiak, B. Papánková, F. Renz, M. Vrbová, R. Werner, Inorg. Chem. 40 (2001) 3025.
[102] (a) J. McMurtrie, I. Dance, CrystEngComm 7 (2005) 230;
(b) J. McMurtrie, I. Dance, CrystEngComm 11 (2009) 1141.
[103] J. Jung, G. Schmitt, L. Wiehl, A. Hauser, K. Knorr, H. Spiering, P. Gütlich, Z. Phys. B: Condens. Matter 100 (1996) 523.
[104] A. Hauser, Coord. Chem. Rev. 111 (1991) 275.
[105] J.-F. Létard, L. Capes, G. Chastanet, N. Moliner, S. Létard, J.-A. Real, O. Kahn, Chem. Phys. Lett. 313 (1999) 115.
[106] S. Marcén, L. Lecren, L. Capes, H.A. Goodwin, J.-F. Létard, Chem. Phys. Lett. 358 (2002) 87.
[107] C. Enachescu, J. Linares, F. Varret, K. Boukheddaden, E. Codjovi, S.G. Salunke, R. Mukherjee, Inorg. Chem. 43 (2004) 4880.
[108] (a) G. Chastanet, C. Carbonera, C. Mingotaud, J.-F. Létard, J. Mater. Chem. 14 (2004) 3516;
(b) H.Z. Lazar, T. Forestier, S.A. Barrett, C.A. Kilner, J.-F. Létard, M.A. Halcrow, Dalton Trans. (2007) 4276.
[109] (a) L. Capes, J.-F. Létard, O. Kahn, Chem. Eur. J. 6 (2000) 2246;
(b) C. Baldé, C. Desplanches, A. Wattiaux, P. Guionneau, P. Gütlich, J.-F. Létard, Dalton Trans. (2008) 2702;
(c) J.-F. Létard, M. Kollmansberger, C. Carbonera, M. Marchivie, P. Guionneau, C. R. Chimie 11 (2008) 1155;
(d) B. Weber, E. Kaps, J. Weigand, C. Carbonera, J.-F. Leĭtard, K. Achterhold, F.G. Parak, Inorg. Chem. 47 (2008) 487;

(e) V. Mishra, R. Mukherjee, J. Linares, C. Balde, C. Desplanches, J.-F. Létard, E. Collet, L. Toupet, M. Castro, F. Varret, Inorg. Chem. 47 (2008) 7577;
(f) S. Hayami, K. Hiki, T. Kawahara, Y. Maeda, D. Urakami, K. Inoue, M. Ohama, S. Kawata, O. Sato, Chem. Eur. J. 15 (2009) 3497.
[110] (a) J. Kusz, H. Spiering, P. Gütlich, J. Appl. Crystallogr. 34 (2001) 229;
(b) M. Marchivie, P. Guionneau, J.A.K. Howard, G. Chastanet, J.-F. Létard, A.E. Goeta, D. Chasseau, J. Am. Chem. Soc. 124 (2002) 194;
(c) E.J. MacLean, C.M. McGrath, C.J. O'Connor, C. Sangregorio, J.M.W. Seddon, E. Sinn, F.E. Sowrey, S.J. Teat, A.E. Terry, G.B.M. Vaughan, N.A. Young, Chem. Eur. J. 9 (2003) 5314;
(d) A.L. Thompson, A.E. Goeta, J.A. Real, A. Galet, M.C. Muñoz, Chem. Commun. (2004) 1390;
(e) V. Niel, A.L. Thompson, A.E. Goeta, C. Enachescu, A. Hauser, A. Galet, M.C. Muñoz, J.A. Real, Chem. Eur. J. 11 (2005) 2047;
(f) J. Kusz, D. Schollmeyer, H. Spiering, P. Gütlich, J. Appl. Crystallogr. 38 (2005) 528;
(g) E. Trzop, M. Buron-Le Cointe, H. Cailleau, L. Toupet, G. Molnár, A. Bousseksou, A.B. Gaspar, J.A. Real, E. Collet, J. Appl. Crystallogr. 40 (2007) 158;
(h) V. Legrand, S. Pillet, C. Carbonera, M. Souhassou, J.-F. Létard, P. Guionneau, C. Lecomte, Eur. J. Inorg. Chem. (2007) 5693;
(i) D. Glijer, J. Hébert, E. Trzop, E. Collet, L. Toupet, H. Cailleau, G.S. Matouzenko, H.Z. Lazar, J.-F. Létard, S. Koshihara, M. Buron-Le Cointe, Phys. Rev. B 78 (2008) 134112;
(j) C.-F. Sheu, K. Chen, S.-M. Chen, Y.-S. Wen, G.-H. Lee, J.-M. Chen, J.-F. Lee, B.-M. Cheng, H.-S. Sheu, N. Yasuda, Y. Ozawa, K. Toriumi, Y. Wang, Chem. Eur. J. 15 (2009) 2384.
[111] V. Legrand, S. Pillet, H.-P. Weber, M. Souhassou, J.-F. Létard, P. Guionneau, C. Lecomte, J. Appl. Crystallogr. 40 (2007) 1076.
[112] (a) R. Hinek, P. Gütlich, A. Hauser, Inorg. Chem. 33 (1994) 567;
(b) R. Hinek, H. Spiering, D. Schollmeyer, P. Gütlich, A. Hauser, Chem. Eur. J. 2 (1996) 1427;
(c) N.O. Moussa, G. Molnár, X. Ducros, A. Zwick, T. Tayagaki, K. Tanaka, A. Bousseksou, Chem. Phys. Lett. 402 (2005) 503.
[113] G.S. Matouzenko, J.-F. Létard, S. Lecoeq, A. Bousseksou, L. Capes, L. Salmon, M. Perrin, O. Kahn, A. Collet, Eur. J. Inorg. Chem. (2001) 2935.
[114] (a) E.C. Constable, Adv. Inorg. Chem. Radiochem. 30 (1986) 69;
(b) E. Baranoff, J.-P. Collin, L. Flamigni, J.-P. Sauvage, Chem. Soc. Rev. 33 (2004) 147;
(c) H. Hofmeier, U.S. Schubert, Chem. Soc. Rev. 33 (2004) 373;
(d) E.C. Constable, Chem. Soc. Rev. 36 (2007) 246.
[115] L.J. Barbour, J. Supramol. Chem. 1 (2003) 189.
[116] POVRAY v. 3.5, Persistence of Vision Raytracer Pty. Ltd., Williamstown, Victoria, Australia, 2002, http://www.povray.org.
[117] F.H. Allen, Acta Crystallogr. Sect. B 58 (2002) 380.
[118] SIGMAPLOT, v. 8.02, SPSS Scientific Inc., Chicago, IL, USA, 2002.